AFGL-TR-85-0008

A STUDY OF THE CHEMISTRY OF ALKALI METALS IN THE UPPER ATMOSPHERE

J.A. Silver
C.E. Kolb

Aerodyne Research, Inc.
45 Manning Road
Billerica, Massachusetts 01821

Scientific Report No. 2

January 1985

AIR FORCE GEOPHYSICS LABORATORY
AIR FORCE SYSTEMS COMMAND
UNITED STATES AIR FORCE
HANSCOM AFB, MASSACHUSETTS 01731

This technical report has been reviewed and is approved for publication.

Charles C. Gallagher

CHARLES C. GALLAGHER
Contract Manager

William Swider

WILLIAM SWIDER, Acting Chief
Ionospheric Disturbances Branch

FOR THE COMMANDER

Robert A. Skrivanek

ROBERT A. SKRIVANEK, Director
Ionospheric Physics Division

This report has been reviewed by the ESD Public Affairs Office (PA) and is releasable to the National Technical Information Service (NTIS).

Qualified requestors may obtain additional copies from the Defense Technical Information Center. All others should apply to the National Technical Information Service.

If your address has changed, or if you wish to be removed from the mailing list, or if the addressee is no longer employed by your organization, please notify AFGL/DAA, Hanscom AFB, MA 01731. This will assist us in maintaining a current mailing list.

Accession For	
NTIS GRA&I	X
DTIC TAB	☐
Unannounced	☐
Justification	
By	
Distribution/	
Availability Codes	
Dist	Avail and/or Special
A/1	

UNCLASSIFIED

SECURITY CLASSIFICATION OF THIS PAGE (When Data Entered)

REPORT DOCUMENTATION PAGE		READ INSTRUCTIONS BEFORE COMPLETING FORM
1. REPORT NUMBER AFGL-TR-85-0008	2. GOVT ACCESSION NO.	3. RECIPIENT'S CATALOG NUMBER
4. TITLE (and Subtitle) A STUDY OF THE CHEMISTRY OF ALKALI METALS IN THE UPPER ATMOSPHERE		5. TYPE OF REPORT & PERIOD COVERED Scientific Report No. 2 6. PERFORMING ORG. REPORT NUMBER ARI-RR-441
7. AUTHOR(s) J.A. Silver and C.E. Kolb		8. CONTRACT OR GRANT NUMBER(s) F19628-83-C-0010
9. PERFORMING ORGANIZATION NAME AND ADDRESS Aerodyne Research, Inc. 45 Manning Road Billerica, MA 01821		10. PROGRAM ELEMENT, PROJECT, TASK AREA & WORK UNIT NUMBERS 61102F 2310G3AY
11. CONTROLLING OFFICE NAME AND ADDRESS Air Force Geophysics Laboratory Hanscom AFB, MA 01731 Monitor/Charles Gallagher/LID		12. REPORT DATE January 1985 13. NUMBER OF PAGES 70
14. MONITORING AGENCY NAME & ADDRESS (if different from Controlling Office)		15. SECURITY CLASS. (of this report) UNCLASSIFIED 15a. DECLASSIFICATION/DOWNGRADING SCHEDULE

16. DISTRIBUTION STATEMENT (of this Report)

Approved for public release; distribution unlimited

17. DISTRIBUTION STATEMENT (of the abstract entered in Block 20, if different from Report)

18. SUPPLEMENTARY NOTES

19. KEY WORDS (Continue on reverse side if necessary and identify by block number)

reaction rates
atomic sodium
mesospheric chemistry
stratospheric chemistry
diffusion
sodium hydroxide
hydrochloric acid
ozone

20. ABSTRACT (Continue on reverse side if necessary and identify by block number)

The reactions of metallic species introduced into the atmosphere by meteor ablation may play a significant role in mesospheric and stratospheric chemistry. During this second year of a three year program to investigate these phenomena, we have completed measurements for the reactions of atomic sodium with ozone, and of NaO with ozone. Preliminary measurements of the rate constant for the reaction of NaO_2 + HCl have been done, as well as an initial photodissociation cross section determination for NaCl at 193 nm. We have also begun to

DD FORM 1 JAN 73 1473

UNCLASSIFIED

SECURITY CLASSIFICATION OF THIS PAGE (When Data Entered)

Cont'd

UNCLASSIFIED

SECURITY CLASSIFICATION OF THIS PAGE(When Data Entered)

investigate the means by which neutral gas phase alkali species may be removed from the mesosphere and stratosphere. Originator Supplied Keywords include:

(U.U.173) (Block 19)

UNCLASSIFIED

SECURITY CLASSIFICATION OF THIS PAGE(When Data Entered)

TABLE OF CONTENTS

1. OBJECTIVE

1.1 Introduction

Metallic elements volatilized during meteor entry into the Earth's upper atmosphere play a significant role in the structure of the D and E regions of the ionosphere,[1-2] and, at least in the case of sodium, the visible day and nightglow emissions from the mesosphere and lower thermosphere.[3-5] Recently, it was suggested that sodium and other meteor metals may be important in stratospheric chemistry by affecting ozone reduction by the catalytic chlorine cycle.[6-8]

The influx of meteor metals into the upper atmosphere has been estimated[9] to be 3.5×10^6 kg yr^{-1}, with a sodium abundance of 2% leading to a calculated sodium flux of 1.2×10^4 atoms cm^{-2} s^{-1}. Other estimates of sodium flux run as high as 2×10^4 cm^{-2} s^{-1}.[10] The flux of other metallic species such as Mg, Ca, Al, Si and Fe will be as much as 10 times higher and speculative concerns about their influence on upper atmospheric homogeneous and heterogeneous chemistry have been published.[1-2,7-8,10]

Unfortunately, all attempts to model the role of volatilized meteor metals (particularly sodium) in the mesosphere and stratosphere[3-4,7,19-15] have suffered from an almost total lack of measured rate constants. All such models start with the oxidation of sodium or other metallic species in reaction with atmospheric O, O_2, or O_3. Until 1982, the only measured chemical rate constants available for any meteor metal oxidation reactions were the three body recombination reactions of alkali atoms (Na, K) with O_2[16-18]

$$\text{Na or K} + O_2 + M \rightarrow NaO_2 \text{ or } KO_2 + M \quad . \qquad (1)$$

Flame studies by Hynes et al[17] and direct measurements at lower temperatures by Husain and Plane[16] showed that this reaction rate is 1000 times faster than previously believed.[19-20] Recent direct flow tube measurements[18] in our laboratory have extended these results from 700 K down to 300 K, and show that the reaction rates vary inversely with temperature, and confirm the larger values for the rate constants.

As an indication of the effect that the availability of chemical rate data has on aeronomic modeling studies, consider the theoretical calculation of several important sodium oxidation reaction rate constants:

$$Na + O_3 \rightarrow NaO + O_2 \quad (2)$$

$$NaO + O \rightarrow Na + O_2 \quad (3)$$

and

$$NaO + O_3 \rightarrow \text{Products} \quad (4)$$

performed at Aerodyne Research, Inc.[21] The adoption of realistic values for just these three rate constants has led to a major revision in the understanding of the structure of the mesospheric sodium layer,[22] the magnitude of the sodium D line nightglow,[5,21] and the understanding of long-lived luminous meteor trails.[8,21]

From the recent modeling work[7-8,10,13,21-22] and comparison of these models with atmospheric measurements,[12,14-15] neutral sodium is believed to be transformed via a series of chemical reactions involving NaO, NaO_2, and NaOH. A survey of the relevant literature[6-8,10,13] provides a fairly complete list of possible neutral sodium reactions of importance. These are listed in Table 1.1, in four groups, which to some extent, reflect the sequence of events from the introduction of neutral sodium at 110 km altitude to its disappearance near 70 km. Also listed are reaction anthalpies, with associated uncertainties.

Table 1.1 - Atmospheric Reactions of Neutral Sodium Species

		$-\Delta H°_r$(kJ mol^{-1})
I. Sodium Atom Reactions		
$Na + O_2 \xrightarrow{M}$	NaO_2	163 ±21
$Na + O_3 \rightarrow$	$NaO + O_2$	167 ±42
$Na + HO_2 \rightarrow$	$NaOH + O$	77 ±15
	$NaH + O_2$	4 ±21
	$NaO + OH$	
$Na + O \xrightarrow{M}$	NaO	273 ±42
II. Sodium Oxide Reactions		
$NaO + O_3 \rightarrow$	$NaO_2 + O_2$	282 ±47
	$Na + 2O_2$	119 ±42
$NaO + H_2O \rightarrow$	$NaOH + OH$	1 ±44
$NaO + H_2 \rightarrow$	$NaOH + H$	64 ±44
$NaO + CH_4 \rightarrow$	$NaOH + CH_3$	61 ±44
$NaO + HCl \rightarrow$	$NaCl + OH$	134 ±42
$NaO + O \rightarrow$	$Na + O_2$	22 ±42
$NaO + HO_2 \rightarrow$	$NaOH + O_2$	30 ±44
$NaO + H \rightarrow$	$Na + OH$	155 ±42
$NaO + ClO \rightarrow$	$NaOCl + O$	
$NaO_2 + HCl \rightarrow$	$NaCl + HO_2$	13 ±23
$NaO_2 + Cl \rightarrow$	$NaCl + O_2$	247 ±21
$NaO_2 + ClO \rightarrow$	$NaCl + O_3$	84 ±21
$NaO_2 + H_2 \rightarrow$	$NaOH + OH$	103 ±24
	$NaO + H_2O$	103 ±47
$NaO_2 + O \rightarrow$	$NaO + O_2$	110 ±47
$NaO_2 + OH \rightarrow$	$NaOH + O_2$	181 ±24
$NaO_2 + H \rightarrow$	$NaOH + O$	111 ±24
	$Na + HO_2$	34 ±23
III. Sodium Hydroxide Reactions		
$NaOH + HCl \rightarrow$	$NaCl + H_2O$	133 ±13
$NaOH + Cl \rightarrow$	$NaCl + OH$	67 ±13
$NaOH + ClO \rightarrow$	$NaCl + HO_2$	63 ±15
$NaOH + H \rightarrow$	$Na + H_2O$	154 ±13
$NaOH + CO_2 \xrightarrow{M}$	$NaHCO_3$	
$NaOH + HNO_3 \rightarrow$	$NaNO_3 + H_2O$	
$NaHCO_3 + HCl \rightarrow$	$NaCl +$ Products	
IV. Photolysis Reactions		
$NaOH + h\nu \rightarrow$	$Na + OH$	
$NaO + h\nu \rightarrow$	$Na + O$	
$NaO_2 + h\nu \rightarrow$	$Na + O_2$	
$NaCl + h\nu \rightarrow$	$Na + Cl$	

The main removal mechanisms of sodium are by reaction with O_2 or O_3, the latter reaction used by Chapman[23] to describe the Na nightglow. The recent rate measurements of reaction (1) however, lead us to believe that below 80 km most of the Na is converted to NaO_2.

The fate of NaO_2, however, is uncertain. Recent measurements by Figger et al[24] and flame studies by Hynes et al[17] imply that the $Na-O_2$ bond strength is much weaker than previously believed, with a value of ca. 163 kJ mol^{-1}. As a result, NaO_2 will react exothermically with atomic oxygen to produce NaO. Sodium oxide can react either with ozone to reform NaO_2 or react with water to produce NaOH.

$$NaO_2 + O \rightarrow NaO + O_2 \qquad (5)$$

$$NaO + O_3 \rightarrow NaO_2 + O_2 \qquad (6)$$

$$NaO + H_2O \rightarrow NaOH + OH \qquad (7)$$

Unfortunately at the beginning of this project, none of these rates had been reliably measured, leading the various modelers to speculate on the importance of each.[10,12-15] As shown by Sze et al,[13] the predominant alkali species below 70 km may be NaO, NaO_2, and/or NaOH, depending on ones choice for k_5, k_6, and k_7.

In a recent paper by Murad et al,[8] it was proposed that the reactions of metal hydroxides and superoxides with chlorine compounds between 40 and 70 km may have an impact on the depletion of stratospheric ozone. In the case of sodium, the exothermic bimolecular reactions

$$NaOH + HCl \rightarrow NaCl + H_2O \quad , \qquad (8)$$

$$NaOH + ClO \rightarrow NaCl + HO_2 \quad , \qquad (9)$$

$$NaOH + Cl \rightarrow NaCl + OH \quad (10)$$

$$NaO_2 + HCl \rightarrow NaCl + HO_2, \quad (11)$$

$$NaO_2 + ClO \rightarrow NaCl + O_3, \quad (12)$$

$$NaO_2 + Cl \rightarrow NaCl + O_2 \quad (13)$$

might be expected to proceed rapidly and act as a sink for Cl, given that NaCl can readily polymerize and condense via heterogeneous nucleation.[8] Murad et al calculated that if the reaction rate of these sodium species with HCl were $\sim 10^{-11}$ cm^3 $molecule^{-1}$ s^{-1}, they might be comparable to the major Cl regeneration mechanism,

$$OH + HCl \rightarrow Cl + H_2O \quad . \quad (14)$$

While previously published studies have viewed NaCl as a potential sink for stratospheric chlorine,[7-8] more recent analyses by F.S. Rowland[25] indicate that photolysis of NaCl may in fact release free Cl. Given the potentially large J values (atmospheric photolysis rate) for this process,[25-26] reactions (8)-(13) could effectively supplement, rather than remove, reaction (14) as a release mechanism for Cl from the inactive HCl stratospheric reservoir and thereby determine the extent to which ozone might be depleted by chlorine compounds in the stratosphere. However, to fully understand the role of alkali species in the stratosphere one must also consider the effects of NaO_2 and NaOH photodissociation on those processes,[13,27] as well as homonuclear and heteronuclear sinks for meteoric metal species.

The objective of this work is to provide direct experimental measurements of these key rate constants. Obtaining accurate reaction rates for the sodium atmospheric system will enable more accurate modeling of the sodium emission

and density profiles. Once this is completed, these results can be extended toward the larger goal of understanding the chemistry of the more abundant meteor metals.

During the first year of this program, rate constants for the recombination reactions of alkali atoms with molecular oxygen, $K + O_2 + M \rightarrow KO_2 + M$, and $Na + O_2 + M \rightarrow NaO_2 + M$, were measured as a function of temperature from 300 to 700 K using a fast flow reactor (see Appendix A). Laser induced fluorescence was used to monitor the disappearance of Na or K as a function of O_2 and M. The reactions were studied in their low pressure third order limit from 1 to 7 torr total pressure with N_2, He, and Ar as third bodies, and the rate constants were found to have the expected negative temperature dependence. These results compared well with other recent measurements from flame and flash photolysis studies and with theoretical expectations based on an energy transfer RRKM mechanism for the NaO_2^* activated complex. Similar techniques were used to demonstrate that the reactions of NaO and NaOH with HCl had a gas kinetic rate constant. (Appendix B) In addition, limits for the rate constants were found for the reactions of atomic hydrogen with NaO, NaOH, and NaCl.

The work during this past year has continued and expanded our efforts of the first year. We have measured reaction rate constants for $Na + O_3$ and $NaO + O_3$ at 294 K, and have preliminary data for $NaO_2 + HCl$ and for photodissociation cross sections of NaCl. In addition, we have begun to examine the various ways in which the reaction neutral gas phase alkali species are removed from the mesosphere and stratosphere.

1.2 Work Forecast

During the next year of this program, we will continue our examination of the chemistry of alkali metals in the mesosphere and upper stratosphere. The major reactions of interest are $NaO_2 + HCl$, $NaO + H_2O$ and $NaOH + CO_2 + M$. In addition, we hope to measure photodissociation cross sections for NaOH, NaCl, NaO, and NaO_2.

2. TECHNICAL PROGRESS

2.1 Introduction

We have made good progress during this second year of our program to study the gas phase kinetics of meteoric metals in the atmosphere. In this section, we will describe in detail the experimental results obtained this year and mention our plans for the coming year. The experiments have been performed in the Aerodyne high temperature, fast flow reactor, which has been described in detail previously[18,28-29] and will not be repeated here.

2.2 Measurements of Atomic Sodium and Potassium Diffusion Coefficients

In the process of analyzing experimental kinetic data, it is necessary to make corrections for diffusion in the observed first-order decay rates. In our experiments, the probability of any alkali species sticking to the wall of the flow tube is unity. This fact allowed us (see Appendix C for details) to directly determine diffusion coefficients from observed wall loss measurements, and resulted in a publication in the Journal of Chemical Physics.[30]

The results are shown in Table 2.1.

Table 2.1 - Diffusion Coefficients for Na and K in Various Gases

GASES	D(cm^2 s^{-1} at 1 atm)	T (K)
Na-He	$(2.2\pm0.3) \times 10^{-5}\ T^{1.75\pm0.02}$	309-473
Na-N_2	$(8.0\pm0.8) \times 10^{-6}\ T^{1.79\pm0.02}$	320-698
Na-Ar	$(1.2\pm0.9) \times 10^{-5}\ T^{1.71\pm0.11}$	322-350
K-He	$(1.5\pm1.0) \times 10^{-3}\ T^{1.48\pm0.19}$	301-734
K-N_2	$(4.5\pm2.8) \times 10^{-5}\ T^{1.54\pm0.09}$	302-720

2.3 Reaction Rate Constants for Na and NaO with O_3

2.3.1 Ozone Production and Detection

Measurement of the reaction rate constant of atomic sodium with ozone is straightforward, given a quantifiable source of ozone. The loss rate of atomic sodium is monitored by laser induced fluorescence as discussed previously.[29] In these studies, O_3 is in excess of Na so that a pseudo-first order kinetic analysis can be used.

Ozone is produced in a small commercial ozonator (Welsbach Model T-408) and stored by cryogenic trapping on silica gel in a specially designed trap. Once stored in this trap, ozone is introduced into the flow tube by eluting it with a known flow of helium. The concentration of O_3 in this flow is determined using a compact, calibrated absorption cell, similar in design to that described in Ref. 31. The partial pressure of O_3 is calculated using the measured cross section for the coincidental absorption of the 253.7 nm mercury line, generated in a standard pen lamp. The flow rate of ozone is then

$$\phi_{O_3}(\text{STP cm}^3\text{s}^{-1}) = \left(\frac{P_{O_3}}{P_{total} - P_{O_3}}\right) \phi_{He}\ (\text{STP cm}^3\text{s}^{-1}) \qquad (15)$$

2.3.2 Rate Measurements and Analysis

In preparing to measure the rate constant of the reaction

$$Na + O_3 \rightarrow NaO + O_2 \qquad \Delta H_r^o = -39.9 \text{ kcal/mole}, \qquad (2)$$

it turns out that we must also be aware of possible complications due to secondary reactions of the NaO product,

$$NaO + O_3 \rightarrow Na + 2O_2 \qquad \Delta H_r^o = -28.4 \text{ kcal/mole, and} \qquad (4a)$$

$$NaO + O_3 \rightarrow NaO_2 + O_2 \qquad \Delta H_r^o = -67.4 \text{ kcal/mole.} \qquad (4b)$$

The termolecular combination reaction,

$$Na + O_2 + M \rightarrow NaO_2 + M, \qquad (1)$$

is too slow[2] at the experimental pressures to be of importance. If the products of reaction (4) are $NaO_2 + O_2$, then no complications in analyzing the [Na] decay for k_2 would exist. However, if reaction (4a) plays a significant role, the Na formed in this reaction will subsequently react with O_3, causing the observed [Na]-time profiles to depart from a simple logarithmic decay. An example of predicted behavior for [Na] decays is illustrated in Figure 2-1. In this calculation, assume that $k_2 = 4 \times 10^{-10}$ $cm^3 s^{-1}$ and vary both the value of k_4 and the ratio k_{4a}/k_{4b}. As expected, if $k_{4a} = 0$, then the observed decay corresponds to k_2. If k_{4a} is finite, then the various curves in [Na] will be observed.

The mathematical expression which describes the curves in Figure 1 can be written as

$$[Na(t)] = \frac{(k_4-k_2+A)e^{-[O_3](k_2+k_4-A)t/2} - (k_4-k_2-A)e^{-[O_3](k_2+k_4+A)t/2}}{2A} \qquad (16)$$

where $k_4 = k_{4a} + k_{4b}$ and

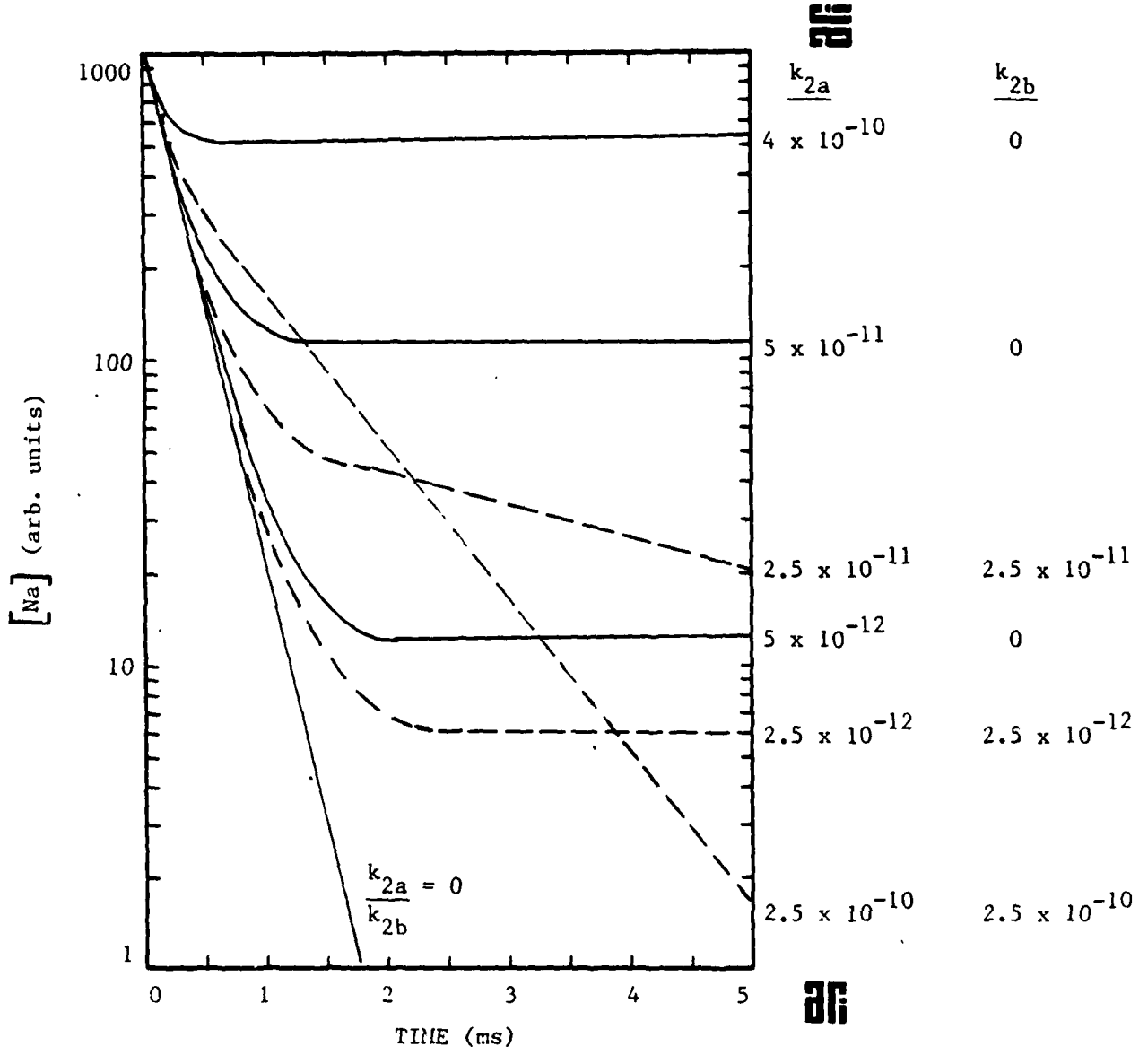

Figure 2-1. Calculated Sodium Profiles for Various Values of k_{4a} and k_{4b}, Assuming $K_2 = 4 \times 10^{-10}$ cm^3 s^{-1}.

$$A = [(k_2 + k_4)^2 - 4k_2k_{4b}]^{1/2}$$

Thus, the Na concentration varies as the sum of two exponential terms whose variables are $[O_3]t$. We can then combine all of our data, plotting the points as log[Na] vs. $[O_3]t$, and obtain estimates of k_{4a} and k_{4b}.

2.3.3 Results

A series of measurements were performed, and curved decay plots were observed, indicating that the value of k_{4a} is not negligible. In order to more accurately obtain k_2, we added an excess of HCl to the flow. This has the effect of suppresing reactions 4a and 4b. The reaction

$$NaO + HCl \rightarrow NaCl + OH \qquad (17)$$

will overwhelm reaction 4 because $k_{17} = 2.8 \times 10^{-10}$ cm^3 molecule^{-1} s^{-1} and [HCl] >> $[O_3]$.[32] We observe very linear decays over many orders of magnitude in signal (Fig. 2-2). Correction of these data for diffusional and wall effects leads to a value of $k_2 = 3.2 \pm 0.4 \times 10^{-10}$ cm^3 molecule^{-1} s^{-1}, where the uncertainty is one standard deviation and includes consideration of both random and systematic errors (Fig. 2-3). A simple prediction for this reaction rate, based on an electron jump model,[33] would predict a value of 4.7 $\times 10^{-10}$ cm^3 molecule^{-1} s^{-1}. A recent measurement[34] using a similar approach as ours obtained a value for k_2 of 7×10^{-10} cm^3 molecule^{-1} s^{-1}. We are in the process of trying to resolve the factor of two difference between these results.

Substituting k_2 into equation (16), we then attempted to fit our data to obtain values for k_{4a} and k_{4b}. Unfortunately, the scatter in the data is too large at this time to get answers to better than a factor of two. As the value of $k_{4a} + k_{4b}$ approaches or exceeds that of k_4, the fit becomes insensitive to value of $k_{2a} + k_{2b}$; especially if $k_{4b} > k_{4a}$. However, based on the overall shape of the curves, we can deduce that $k_{4a} \sim 3k_{4b}$ and that the overall reaction rate constant for $NaO + O_3$ is $>10^{-10}$ cm^3 molecule^{-1} s^{-1}.

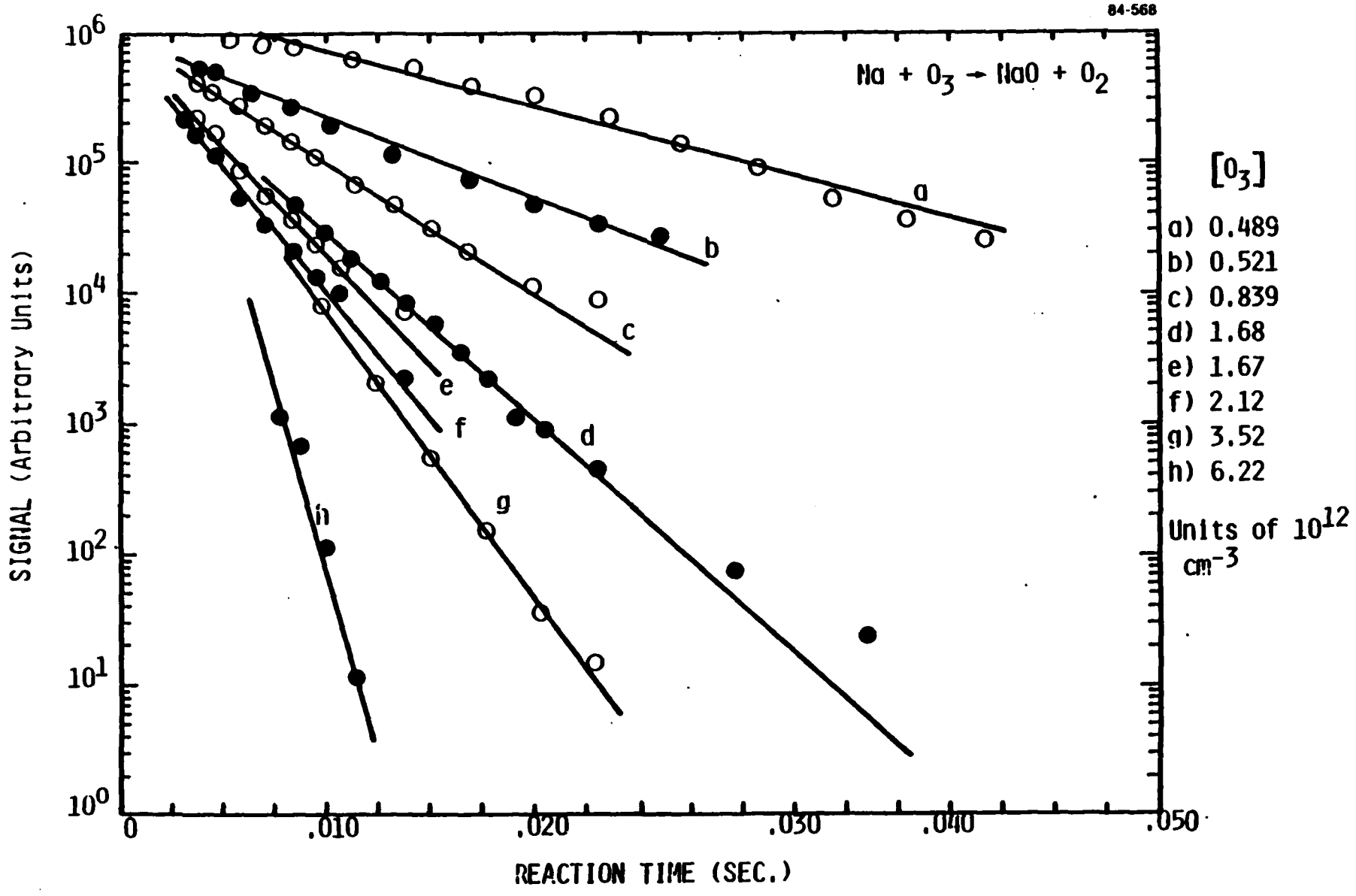

Figure 2-2. Variation of Sodium Fluorescence Signals vs. Reaction Time for Various Ozone Concentrations.

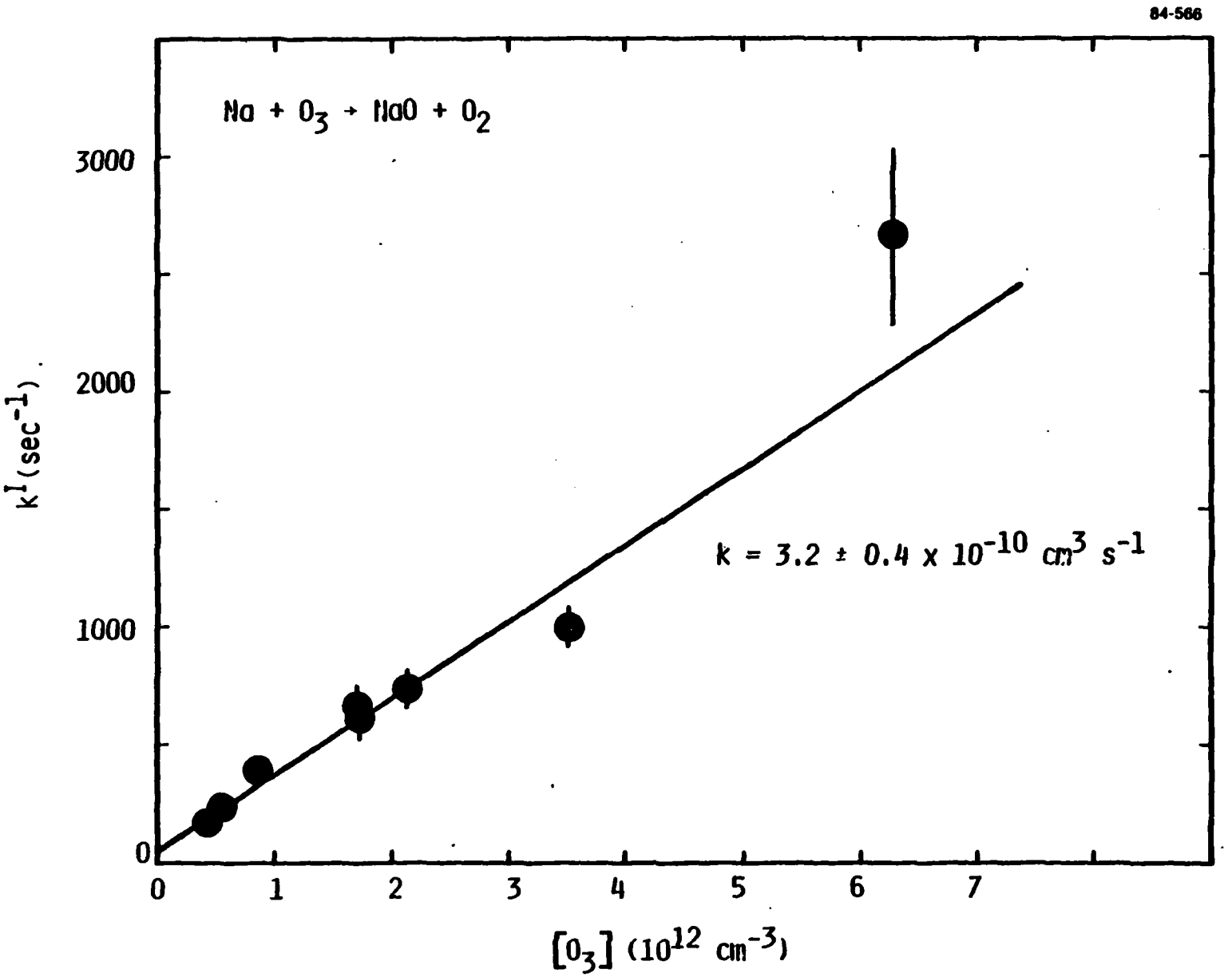

Figure 2-3. Plot of Pseudo-First Order Decay Constant vs. Ozone Concentration.

2.4 Rate Constant for NaO_2 + HCl

We have begun measurements to determine the rate constant for the reaction

$$NaO_2 + HCl \rightarrow NaCl + HO_2 \qquad (11)$$

Sodium superoxide is formed in the upstream region of the flow tube by the termolecular reaction

$$Na + O_2 \xrightarrow{M} NaO_2, \qquad (1)$$

and is detected in a manner described in Appendix B, whereby the NaO_2 is titrated in the detector region by atomic hydrogen, and the resulting sodiumn atom detected by laser-induced fluorescence.

$$NaO_2 + H \rightarrow Na + HO_2 \qquad (18)$$

$$Na + h\nu \rightarrow Na^* \rightarrow Na + h\nu \qquad (LIF) \qquad (19)$$

Because the NaCl product also forms Na upon addition of H,

$$NaCl + H \rightarrow Na + HCl, \qquad (20)$$

(albeit at a slower rate), the observed decay plots are curved and eventually level off at a value reflecting the relative rate constants of reactions 18 and 20.

Preliminary results indicate that the reaction of NaO_2 with HCl is relatively fast. Although more experiments are needed, at this time a lower limit of k can be set at 3×10^{-11} cm^3 $molecules^{-1}$ s^{-1} at 294 K.

2.5 Photodissociation Cross Sections for NaCl

2.5.1 Introduction

If alkali chemistry is going to have an impact on ozone reduction in the upper stratosphere, three criteria must be met: 1) Na must be rapidly

transformed to NaCl, 2) photolysis must quickly regenerate free Cl and atomic Na from NaCl, and 3) homogeneous and heterogeneous processes which remove the mononeric neutral gas phase alkali molecules must not be too rapid. It appears that the first criteria is met, and we will discuss the third in the next section of this report. The photodissociation cross sections of alkali molecules, and most importantly NaCl, need to be measured accurately between approximately 200 nm and 300 nm, the latter value corresponds to just below the dissociation band energy of NaCl.

Although a few previous measurements of alkali halide photoabsorption cross sections have been made,[35-37] they all (with one exception[37] for CsI), have been done at higher temperatures, where dimers and/or vibrational hot bands may have significantly contributed to the observed spectra. Since the photolysis rate is a convolution of the solar spectrum (as seen in the upper stratosphere) and the photodissociation cross section, it is desireable to have detailed cross sections which are free of the effect of dimers and correspond to a stratospheric vibrational temperature of 250 K. Our approach of making NaCl at room temperature by the chemical reaction of Na + Cl_2 more closely satisfies these requirements and should result in an accurate determination of the stratospheric photolysis rate of NaCl.

2.5.2 Experimental Approach and Preliminary Results

Sodium chloride is formed by the rapid reaction of Cl_2 + Na. We have measured this rate constant to be ~6 x 10^{-10} cm^3 $molecule^{-1}$ s^{-1} at 294 K. Our initial approach toward measuring the cross section was to use a high intensity Xe lamp, dispersed through a monochromator, as our light source. As NaCl flowed through an irradiated region, it would photodissociate and the amount of detected Na just downstream relative to the initial amount of NaCl will be expressed as

$$\frac{[Na]_d}{[NaCl]_o} = 1-e^{-\sigma(\lambda)I_o(\lambda)t} \qquad (21)$$

where I_o = photons cm^3 s^{-1} at wavelength λ

$\sigma(\lambda)$ = cross section in cm^2 at λ

t = irradiation time in seconds = iradiation length (d)/gas velocity ($\bar{v}$)

Thus a measurement of the left-hand side of equation 21, coupled with an accurate measurement of I_o, d, and $\bar{v}$, would result in $\sigma(\lambda)$.

Several problems arose, however, in performing these measurements. First, the geometry of the flow tube is such that the flow velocity in the detection region is not equal to that in the reaction portion. Although this has no effect on kinetic measurements, it means that the flow velocity in this region is not easily calculated, but must be measured. Although possible by a variety of techniques, it requires additional work. The second, more serious problem was the Xe illuminator. The 500 Watt lamp we had was incapable of being focussed properly through the monochromator without losing too much intensity. Although a smaller 75 Watt lamp of the proper design was used, it was too weak to provide measureable dissociation cross sections.

After considering the alternate choice of acquiring a new 1000 Watt lamp, we decided to instead go to a laser photolysis setup. In this arrangement, a Raman shifted excimer laser will replace the Xenon lamp. This approach has several advantages. The laser pulse is only about 10 ns long, so that the NaCl molecules are effectively stationary during photolysis. Thus only the total photon density in each pulse is required to be known (i.e., pulse energy and laser beam diameter); we no longer need to know $\bar{v}$. Secondly, instantaneous pulse energy is higher at any selected wavelength, so that $[Na]_d/[NaCl]_o$ will be larger and more easily measured ($\sim 10^{-2} - 10^{-3}$ rather than $10^{-4} - 10^{-6}$ with the 500 W Xe lamp). The probe visible laser is now coincident with the pump (UV) laser and detects the photodissociated Na within a microsecond of formation. NaCl is measured by turning the Cl_2 and excimer laser off, making the assumption that all of the original sodium is

completly converted to NaCl upon addition of excess Cl_2. Since the experiment is over in <1 μs, there is insufficient time for the newly formed sodium atoms to react with this remaining Cl_2 before they are detected. Using H_2/D_2 mixtures in the Raman cell, we can easily cover the 200-300 nm region with at least 25 wavelengths.

At this time we have demonstrated the viability of this approach using the excimer laser alone at 193 nm. Preliminary analysis gives $\sigma = (1.3 \pm 0.6) \times 10^{-17}$ cm^2 at this wavelength. Preparations are now underway for extending these measurements to 300 nm using the Raman shifter.

2.6 Atmospheric Sinks for Meteoric Alkali Compounds

As demonstrated above, alkali gas phase chemistry may significantly impact chlorine induced ozone depletion if 0.1-1% of the potential stratospheric alkali content remains in monomeric molecular form.

Various sinks for gaseous alkalis can be considered. Let us look at three potential sinks for neutral alkali species:

2.6.1 Ionization/Cluster Formation

Hydration of alkali species by $H_3O^+ \cdot nH_2O$ ions will remove neutral alkali and form ions which rapidly cluster and/or condense on aerosols.

$$NaX + H_3O^+ \cdot nH_2O \rightarrow NaXH^+ \cdot nH_2O + H_2O \quad (22)$$

$$NaXH^+ \cdot nH_2O + NaX \rightarrow (NaX)_2 \cdot (n-1)H_2O + H_2O \quad (23)$$

$$[NaX][H_2O] \geq 1/K_{EQ} (23) \quad (24)$$

Upper stratospheric balloon-borne mass spectrometer measurements by Arnold et al[38] and Arijs et al[39] show no identifiable $NaXH^+ \cdot nH_2O$ peaks, thus setting limits on the amount of neutral alkali present. Subject to better refinements of K_{EQ} and mass spectrometer sensitivities, this present limit is not incompatible with an NaX of ~10^4 cm^{-3}.[40] Furthermore, the photolytic

stability of either ion or neutral clusters to reform NaX is unknown. Recent unpublished results from rocket launched, parachute deployed mass spectroscopy measurements of upper stratospheric and lower mesospheric ion measurements by Arnold do indicate a strong possibility of either sodium or magnesium core ions in the 40 to 60 km range.[41]

2.6.2 Homogeneous Condensation

Dimerization and subsequent clustering of alkali species will remove them from the catalytic Cl regeneration cycle discussed above. At night, the alkalis will probably reside in the form of NaCl, which in the absence of light will dimerize.

$$NaCl + NaCl \rightarrow (NaCl)_2$$

Even with an extremely fast termolecular recombination rate of 10^{-28} cm^6 $molecule^{-2}$ s^{-1}, more than 5×10^3 cm^{-3} NaCl will still be in the monomeric form after 4 months, which is the upper limit of estimated replacement time of sodium in the stratosphere by diffusion ($10^6 - 10^7$ s).[42]

2.6.3 Heterogeneous Condensation

It has been suggested by Hunten and co-workers[42] that ablation of meteors may lead the formation of high altitude "smoke", small particles with an integrated equivalent surface area (a) of 10^{-9} cm^2/cm^3 between 30 and 85 km. As the alkali species diffuse downward, they might condense on these aerosols and be removed from the gas phase. The amount of loss depends critically on the accommodation (sticking) coefficient, α, and on the residence time in the atmosphere between 85 and 30 km.

$$(NaX) = (NaX)_o e^{-\alpha avt}$$

With gas-particle relative velocities (v) of $\sim 3 \times 10^4$ cm s^{-1}, $[NaX]/[NaX]_o$ ranges from 0-0.7 for α in the range 1.0-0.01 and $t = 10^6$-10^7 s. Not only are

the accommodation coefficients unknown, but the net loss also depends on whether surface photolysis and/or chemistry releases adsorbed NaX species.

2.7 Summary

In the first two years of this program, much has been learned about the processes governing the chemistry of meteoric metal in the atmosphere. The chemical fate of Na in the lower thermosphere is being clarified due to our results on $Na + O_2 + M$, $Na + O_3$, and $NaO + O_3$. Further work on $NaO + H_2O$ and $NaOH + CO_2 + M$, as well as loss mechanisms, should provide a firm basis for predicting species profiles. The stratospheric chemistry of meteor metals has been better understood due to our results for NaO, NaOH, and NaO_2 with HCl. Further work in this area will involve the determination of photodissociation cross sections for the alkali oxides, hydroxides, and halides.

3. REFERENCES

1. Murad, E., J. Geophys. Res. 83, 5525 (1978).

2. Brown, T.L., Chem. Rev. 73, 645 (1973).

3. Blamont, J.E. and Donahue, T.M., J. Geophys. Res. 69, 4093 (1964).

4. Hunten, D.M., Space Sci. Rev. 6, 493 (1967).

5. a) Kirchhoff, V.W.J.H., Clemesha, B.R., and Simonich, D.M., J. Geophys. Res. 84, 1323 (1979);
   b) Bates, D.R. and Ojha, P.C., Nature 286, 790 (1980).

6. Ferguson, E.E., Geophys. Res. Lett. 5, 1035 (1978).

7. Murad, E. and Swider, W., Geophys. Res. Lett. 6, 929 (1979).

8. Murad, E., Swider, W., and Benson, S.W., Nature 289, 273 (1981).

9. Richter, E.S. and Sechrist, C.F., Jr., J. Atmos. and Terres. Phys. 41, 579 (1979), Geophys. Res. Lett. 6, 183 (1979).

10. Liu, S.C. and Reid, G.C., Geophys. Res. Lett. 6, 283 (1979).

11. a) Baggaley, W.J., Nature 257, 567 (1975);
    b) Baggaley, W.J., Nature 267, 376 (1977);
    c) Hapgood, M.A., Nature 286, 582 (1980.

12. Kirchhoff, V.W.J.H., Clemesha, B.R., and Simonich, D.M., J. Geophys. Res. 86, 6892 (1981).

13. Sze, N.D., Ko, M.K.W., Swider, W., and Murad, E., Geophys. Res. Lett. 9, 1187 (1982).

14. Kirchhoff, V.W.J.H., Geophys. Res. Lett. 10, 721 (1983).

15. Thomas, L., Isherwood, M.C., and Bowman, M.R., J. Atm. Terrestrial Phys. 45, 587 (1983).

16. Husain, D. and Plane, J.M.C., J. Chem. Soc. Far. Trans. 2, 78, 163 (1982); Husain. D, Marshall, P., Plane, J.M.C., J. Chem. Soc. Faraday Trans. 2, 80, 1308 (1984).

17. Hynes, A.J., Steinberg, M., and Schofield, K., J. Chem. Phys. 80, 2585 (1984).

18. Silver, J.A., Zahniser, M.S., Stanton, A.C., and Kolb, C.E., 20th (Int.) Symposium on Combustion, to be published (1984).

19. Carabetta, R. and Kaskan, W.E., J. Phys. Chem. 72, 2483 (1968).

20. McEwan, M.J. and Phillips, L.F., Trans. Faraday Soc. 62, 717 (1966).

21. Kolb, C.E. and Elgin, J.B., Nature 263, 488 (1976).

22. Simonich, D.M., Clemesha, B.R., and Kirchoff, V.W.J.H., J. Geophys. Res. 84, 1543 (1979).

23. Chapman, S., Astrophys. J. 90, 309 (1939).

24. Figger, H., Schrepp, W. and Zhu, Xu-hui, J. Chem. Phys. 79, 1 (1983).

25. Rowland, F.S. and Rogers, P.J., Proc. Natl. Acad. Sci. USA 79 (1982).

26. Davidovits, P. and Brodhead, D.C., J. Chem. Phys. 46, 2968 (1967).

27. Rowland, F.S. and Makide, Y., Geophys. Res. Lett. 9, 473 (1982) and references therein.

28. Gersh, M.E., Silver, J.A., Zahniser, M.S., Kolb, C.E., Brown, R.G., Gozewski, C.M., Kallelis, S., and Wormhoudt, J.C., Rev. Sci. Instrum., 52, 1213 (1981).

29. Silver, J.A., Zahniser, M.S., Kolb, C.E., and Stanton, A.C., "First Annual Technical Report on a Study of Atmospheric Reactions of Neutral Sodium Species and Other Metals of Meteoric Origin", Aerodyne Research Report No. ARI-RR-385 (January, 1984).

30. Silver, J.A., J. Chem. Phys., 81, 5125 (1984).

31. Zahniser, M.S. and Howard, C.J., J. Chem. Phys., 73, 1620 (1980).

32. Silver, J.A., Stanton, A.C., Zahniser, M.S., and Kolb, C.E., J. Phys. Chem., 88, 3123 (1984).

33. Levine, R.D. and Bernstein, R.B., Molecular Reaction Dynamics, p. 86, Oxford University Press, New York, 1974.

34. Howard, C., U. Colorado, private communication, 1984.

35. Davidovits, P. and Brodhead, D.C., J. Chem. Phys., 46, 2968 (1967).

36. Daidoji, H., Bunseki Kagaku, 28, 77 (1979).

37. Grossman, L.W., Hust, G.S., Payne, M.G., and Allman, S.G., Chem. Phys. Lett. 50, 70 (1977).

38. Arnold, F. and Henschew, G., Planetary and Space Sci., 30, 101 (1982).

39. Arijs, E., Nevejans, D., and Ingels, J., Nature (London), 303, 314 (1983); Arijs, E., Nevejans, D., Ingels, J., and Frederick, P., Ann. Geophysicae, 1, 163 (1983).

40. Aiken, A.C., Nature (London), 291, 638 (1981).

41. Arnold, F., private communication, October, 1984.

42. Hunten, D.M., Turko, R.P., and Toon, O.B., J. Atmos. Sci., 37, 1342 (1980).

4. PROPERTY AND EQUIPMENT

During the past year, no major property or equipment was purchased.

5. PERSONNEL CHANGES

No personnel changes were made during this past year.

6. PRESENTATIONS, MEETINGS AND TRAVEL

During this past year, the following presentations were made:

"The Reaction Rates of Na + O_2 + M, K + O_2 + M and NaOH + HCl", by J.A. Silver, M.S. Zahniser, A.C. Stanton, and C.E. Kolb, at the 1983 Fall American Geophysical Union meeting in San Francisco, CA on December 7, 1983.

"Atmospheric Chemistry of Meteoric Metals", by J.A. Silver for a colloquium at the Air Force Geophysics Laboratory on April 19, 1984.

"Temperature Dependent Termolecular Reaction Rate Constants for Potassium and Sodium Superoxide Formation", by J.A. Silver, M.S. Zahniser, A.C. Stanton, and C.E. Kolb, at the 20th International Symposium on Combustion in Ann Arbor, MI in July, 1984.

"The Chemistry of Alkali Oxides in the Atmosphere", by J.A. Silver at the XVI Informal Conference on Photochemistry in Cambridge, MA in August, 1984.

"Gas Phase Alkali Chemistry in the Post-Molecular Beam Age", by C.E. Kolb at MIT on 6 November 1984.

7. PUBLICATIONS

"Temperature Dependent Termolecular Reaction Rate Constant for Potassium and Sodium Superoxide Formation", by J.A. Silver, M.S. Zahniser, A.C. Stanton, and C.E. Kolb, 20th Symposium (Int.) on Combustion, The Combustion Institute (1984).

"The Gas Phase Reaction Rate of Sodium Hydroxide with Hydrochloric Acid", J.A. Silver, A.C. Stanton, M.S. Zahniser, and C.E. Kolb, J. Phys. Chem., 88, 3123 (1984).

"Measurement of Atomic Sodium and Potassium Diffusion Coefficients", J.A. Silver, J. Chem. Phys., 81, 5125 (1984).

APPENDIX A

TEMPERATURE DEPENDENT TERMOLECULAR REACTION RATE CONSTANTS FOR POTASSIUM AND SODIUM SUPEROXIDE FORMATION

To be published, 20th Symposium (International) on Combustion, 1984

ARI-RR-381

TEMPERATURE DEPENDENT TERMOLECULAR REACTION RATE CONSTANTS FOR POTASSIUM AND SODIUM SUPEROXIDE FORMATION

Prepared by

J.A. Silver, M.S. Zahniser, A.C. Stanton, and C.E. Kolb
Center for Chemical and Environmental Physics
Aerodyne Research, Inc.
45 Manning Road
Billerica, MA 01821

Prepared for

The 20th Symposium (International) on Combustion
The Combustion Institute
Pittsburgh, PA

January 1984

Subject Matter: Kinetics

ABSTRACT

Rate constants for the recombination reactions of alkali atoms with molecular oxygen, $K + O_2 + M \rightarrow KO_2 + M$ and $Na + O_2 + M \rightarrow NaO_2 + M$, have been measured as a function of temperature from 300 to 700 K using a fast flow reactor. Laser induced fluorescence is used to monitor the disappearance of Na or K as a function of O_2 and M. The reactions are studied in their low pressure third order limit from 1 to 8 torr total pressure with N_2, He, and Ar as third bodies. The rate constants are found to have the expected negative temperature dependence. The values for k ($Na + O_2 + M$) are $(1.9 \pm 0.4) \times 10^{-30} (T/300)^{-1.1 \pm 0.5}$ with M = N_2, $(1.4 \pm 0.3) \times 10^{-30} (T/300)^{-0.9 \pm 0.5}$ with M = He, and $(1.2 \pm 0.3) \times 10^{-30}$ at T = 324 K with M = Ar, all in units of cm^6 $molecules^{-2}$ s^{-1}. The values for the corresponding reactions with potassium are larger than those for sodium with k ($K + O_2 + M$) = $(5.4 \pm 0.2) \times 10^{-30} (T/300)^{-0.56 \pm 0.20}$ with M = N_2, $(2.0 \pm 0.5) \times 10^{-30} (T/300)^{-0.9 \pm 0.5}$ with M = He, and $(3.5 \pm 1.0) \times 10^{-30}$ at T = 300 K with M = Ar. The results are compared with other recent measurements from flame and flash photolysis studies and with theoretical expectations based on an energy transfer RRKM mechanism for the NaO_2^* activated complex.

INTRODUCTION

The chemistry of alkali metals in flames commands our attention for both scholarly and practical reasons. From a scientific standpoint reactions of alkali atoms, with their single valence electron, form a natural test bed to extend our theoretical understanding honed on reactions of atomic hydrogen. Furthermore, the low ionization potentials of alkali atoms open the possibility of electron transfer reaction mechanisms and allow determination of the role of ionic potential surfaces in reaction dynamics. Finally, incredibly sensitive methods of detecting alkali atoms, including hot wire surface ionization, laser induced resonance fluorescence, and laser induced resonance ionization now allow the design of elegant experimental studies for environments ranging from molecular beams to high pressure flames.

From a practical standpoint, gas phase alkali chemistry has long been recognized to be important in flame suppression,[1-5] and is also involved in the conversion of alkali-containing minerals in coal to alkali sulfates.[6-8] These sulfates are a major cause of fouling and corrosion of boiler-tube surfaces, heat exchangers, and turbine blades. Alkali atoms introduced into the atmosphere by meteor ablation also play a role in mesospheric chemistry,[9-12] and it has been suggested[13-14] that alkali molecules may affect stratospheric ozone reduction through the catalytic chlorine cycle.

However, for all the intrinsic theoretical and experimental interest in alkali reactions, our understanding of the gas phase oxidation chemistry of alkali atoms has only recently progressed, first back to, and then beyond the level gained in the 1930's in pioneering sodium diffusion flame studies by Haber and Sachsse[15] and Bawn and Evans.[16] While these low pressure studies of reaction (2) showed it proceeded with a termolecular rate constant in excess of 10^{-30} cm^6 s^{-1}, subsequent work (primarily in the mid 1960's) using flame photometric methods by Kaskan[17-18] and McEwan and Phillips[19-20] indicated much

lower MO_2 formation rates (M=Na,K)[17-19] as well as relatively high dissociation energies for the $M-O_2$ bond (M=Na,Li).[19-20]

Analyses of thermochemical cycles by Herm and Herschbach[21] and Alexander[22] clearly indicated that the values of $M-O_2$ bonds deduced from flame photometric data by McEwan and Phillips were greatly overestimated. This was recently confirmed by Figger and co-workers who analyzed observations of chemiluminescence between crossed molecular beams of alkali dimers and molecular oxygen to yield alkali superoxide bond energies.[23] Reinterpretation of the earlier flame experiments[24] as well as newly performed flame studies[25] are also consistent with lower alkali superoxide bond energies.

The low sodium and potassium termolecular reaction rates deduced from the flame photometry studies[17-19] are also incorrect. Recently published flash photolysis studies over limited temperature ranges for Li (393 and 463 K),[26] Cs (323 K),[27] Na (724 and 844 K),[28] and K (753 and 853 K),[29] as well as flame photometry studies for Na,[25] all clearly show fast termolecular rates for alkali superoxide formation.

In this paper we report termolecular rate constants for superoxide formation of sodium and potassium over a much wider temperature range than previously available, yielding the first clear, direct measurement of the temperature dependence of these processes. Third body dependencies are illustrated by separate measurements for N_2, He and Ar. These measurements were made in a high temperature, fast flow reactor[30] utilizing laser induced resonance fluorescence detection of atomic alkali species. A discussion of these results in terms of their importance in testing termolecular association reaction theory is also presented.

EXPERIMENTAL

The high temperature fast flow reactor used in these experiments has been described in detail previously[30] and is shown in Fig. 1 in the configuration used in this study. Briefly, a 7.26 cm diameter, 120 cm long alumina tube is heated with Kanthal resistance heaters. The helium, argon or nitrogen carrier gas enters the flow tube through two mullite multichannel arrays which both preheat and laminarize the flow upstream of the reaction zone. A sufficient distance (20 cm) is allowed downstream of these arrays for the carrier gas to develop a parabolic flow profile before reaching the reaction zone. Carrier gas flow rates are measured with calibrated rotameters. Total pressures are measured with a capacitance manometer at the downstream end of the reaction zone. Gas temperatures are obtained with a chromel-alumel thermocouple which is movable throughout the reaction zone. The lowest reaction temperatures are slightly above room temperature due to the heating of the carrier gas as it passes over the resistively heated alkali oven. The maximum axial temperature gradient due to this effect over the region in which decay measurements are taken is 10 to 20 degrees depending on flow velocity, pressure, and identity of carrier gas. The temperature at the mid point of the reaction zone as measured by the movable thermocouple is used in the data analysis. Axial profiles are more uniform, ±2 to 5 degrees, at elevated temperatures (> 400 K) where heating is dominated by the flow tube walls and the mullite arrays. Although the apparatus is capable of temperatures up to 1500 K, experimental considerations as described below limited the upper temperature to 700 K for these studies.

Alkali atoms are generated by heating the pure metal in a 25 mm diameter cylindrical silver plated monel oven to a temperature sufficient to obtain a vapor pressure of 10^{-6} to 10^{-4} torr within the oven. The oven is mounted on the end of a movable 13 mm od alumina tube concentric to the main flow tube. The vapor is entrained in a flow of carrier gas and introduced into the flow tube in one of two configurations. For the kinetic measurements with O_2, the oven is placed at a fixed position upstream of the multichannel arrays and the alkali vapor is introduced into the main flow through a 10 cm length of 19 mm diameter silver tubing which passes through the center of the arrays. In the second configuration, the oven is placed downstream of the arrays and is movable throughout the reaction zone to determine the loss of alkali atoms on the reactor walls. The oven temperature is controlled with resistive heating elements independent of the flow tube heaters. Initial alkali atom concentrations in the reaction zone are maintained at less than 10^{10} cm^{-3} by adjusting the oven temperature and the carrier gas flow rate through the oven.

The alkali atoms are detected by laser induced fluorescence at the downstream end of the flow tube. A Molectron DL14 nitrogen pumped dye laser is used to excite the 4s $^2S_{1/2} \rightarrow$ 5p $^2P_{3/2}$ transition at 404.4 nm for potassium or the 3s $^2S_{1/2} \rightarrow$ 3p $^2P_{3/2}$ transition at 589.0 nm for sodium. Fluorescence is collected using a gated phototube and a computer controlled data acquisition system.[30] The signals are averaged over 100 laser pulses after subtracting for nonfluorescent background contributions and normalizing for pulse to pulse fluctuations in laser intensity. Although no direct calibration of the fluorescence signal was attempted, estimates of sensitivity from known phototube and integrator response, measured laser power, and atomic

transition probabilities indicate a detection limit for Na of 10^4 cm^{-3} and for K of 10^6 cm^{-3} using these transitions.

Molecular oxygen is added through a movable loop injector at distances from 10 to 60 cm upstream of the detection region. O_2 flow rates are measured with a calibrated thermal conductivity mass flow meter. The kinetic measurements are conducted under pseudo-first order conditions with $2 \times 10^{14} < [O_2] < 7 \times 10^{15}$ cm^{-3}, in large excess compared to the alkali metal atom concentration, yet always <5% of the total gas concentration. First order rate constants are determined for a fixed O_2 concentration by recording the change in alkali atom concentration as a function of O_2 injector distance.

Corrections for both axial and radial diffusion and wall removal are made using the procedure outlined by Brown.[31] This method is based on a numerical solution of the continuity equation including diffusion, first order chemical reaction and wall removal in a cylindrical tube with fully developed laminar flow. A multiplicative correction factor, obtained for each set of experimental conditions, is used to relate the observed decay to the true first order rate constant. This correction factor is dependent on the wall removal rate constant, k_w, and the binary diffusion coefficient for the alkali atom in the carrier gas. Values for k_w are determined in separate experiments at each pressure and temperature by observing the change in atom concentration at the detection point while varying the source oven position. The loss of atoms to the wall was found to be diffusion limited for all the conditions used in this study, implying a surface accommodation coefficient $\gamma > 0.1$. The observed wall loss rate under these conditions may therefore be used to determine the diffusion coefficient[32] which are then used to determine the correction factors for the reactive flow analysis. The correction factors obtained by this method were in the range k_{true}/k_{obs} from 1.52 to 1.86, with most lying between 1.60 and 1.65. Under the flow conditions of these experiments, the ratio of reaction to diffusion times is not unlike those encountered in ion-molecule reactions,[33] which also exhibit correction factors on the order of 1.6.

RESULTS AND DISCUSSION

Reaction rate constants of atomic sodium with O_2 were measured over the temperature range of 320 - 698 K for nitrogen as the third body collision partner, and over the range of 309 - 473 K in helium; for potassium, the corresponding temperature ranges were 308 - 720 K and 296 - 520 K, respectively. Room temperature measurements were also made in argon for both Na and K. Pressures encompassed at each temperature range from 1 to between 5 and 8 torr. Above 700 K, no reliable decays could be measured, because alkali atoms which had accumulated on the walls at lower temperatures began to effuse into the flow, interfering with the rate measurements.

Using the data for Na + O_2 + (He) as an example, we see in Fig. 2 that the first-order (logarithmic) decays of signal with reaction time are linear for over a factor of 100. Plots of a series of first-order rate constants (corrected for wall and diffusional effects) versus $[O_2]$ are illustrated in Fig. 3. Second-order rate constants derived from these are then plotted vs. total number density and the third-order rate constants are determined from the slopes of these plots. In most cases, these lines intersect the origin to within the statistical uncertainties of the fit ($\pm 10\ s^{-1}$). For Na + O_2 + (N_2), a small positive intercept is observed at all temperatures. The cause for the intercept is unclear. An explanation sometimes given for such behavior is that the wall acts as a stabilizing third body and adds a pressure independent component to k^{II}. However, this explanation would appear unlikely in these experiments given the near unit efficiency for wall removal of all alkali species. An alternative explanation is that insufficient diffusional mixing of the injected O_2 could lead to underestimation of k^{II} at higher pressures, resulting in an apparent intercept in the k^{II} vs. pressure plots. However, calculations of mixing length indicate that this effect should not be significant even at the highest pressure (8 torr) in these studies.

The three-body association rate constants as a function of temperature for various third body collision partners are shown for sodium in Fig. 4 and for potassium in Fig. 5. The data can be described by an expression of the form $k^{III}(T) = AT^{-n}$. The results of nonlinear least-square fits to this function are found in Table I. For sodium in helium and nitrogen, and for potassium in helium, a simple T^{-1} representation could also be used. However, the results for potassium in nitrogen show a somewhat weaker temperature dependence, best represented by $T^{-(0.56 \pm 0.20)}$ although this difference is not significant within the statistical uncertainties of the data.

The expressed total experimental uncertainties, including allowance for systematic errors, can be estimated as the square root of the sum of the squared individual uncertainties due to a) flow velocity, temperature, pressure, and concentration calibration factors, 5%, b) the precision in determining the coefficient A in the expression for $k^{III}(T)$, 17%, and c) the uncertainty in the correction of observed first-order decays for wall removal and diffusional effects, 10%.

Table I also contains other determinations of k_2. Husain and Plane[28-29] used a flash photolysis system to generate alkali atoms from KI and NaI and followed the decay of K and Na by atomic resonance absorption. They observed no temperature dependence over their limited temperature range (724 K and 844 K) for the Na + O_2 + M reaction. A substantially larger variation with temperature was obtained for their K + O_2 + M study although they arbitrarily fit their data to a T^{-1} dependence. The agreement between their values and the slightly extrapolated temperature dependent rate constants for both reactions from this work is satisfactory, especially considering the very different methods employed. This comparison is shown in Figs. 4 and 5.

Hynes et al.[25] have studied the Na + O_2 + M reaction in experiments using laser induced fluorescence to measure Na and OH profiles under fuel lean conditions in $H_2/O_2/N_2$ flames. A detailed kinetic model assuming reasonable values for rate constants for the reactions interconnecting the species Na, NaO_2, NaO and NaOH is used to determine the best fit to the observations.

Their optimum value of k(Na + O_2 + M), assuming a T^{-1} temperature dependence, is shown in Fig. 4, and is lower by about a factor of 4 compared to the extrapolated fit from this work. Part of this difference may be explained by the different identities of M (N_2, O_2, H_2O mixtures) in their flame studies. Hynes et al.[25] also explain the discrepancy between their result and the earlier flame studies,[17-19] which obtained a lower value for k(Na + O_2 + M) by nearly three orders of magnitude. The earlier works had incorrectly attributed the global disappearance of Na to reaction with O_2, while in fact the Na concentration follows that of atomic hydrogen, whose decay is controlled by reaction with O_2 to form HO_2. A similar explanation has been proposed by Jensen.[24]

The much earlier diffusion flame studies[15-16] correctly identified the Na + O_2 + M reaction to be fast for a three body process. The later and more extensive study by Bawn and Evans[16] obtained a value at 533 K which is higher by a factor of 3 than this study. They also observed a fall-off behavior for their second order rate constant with pressure above about 10 torr and present their results in terms of an energy transfer mechanism using a Lindemann-type expression to interpret their data. This fall-off behavior was not observed by Husain and Plane[28] who show linear plots of k_2^{II} versus pressure from 25 to 150 torr. Their effective bimolecular rate at 150 torr and 724 K for the Na + O_2 + (N_2) reaction of 2.2×10^{-12} cm^3 s^{-1} is nearly equal to the high pressure limit inferred by Bawn and Evans of 3×10^{-12} cm^3 s^{-1}. It thus appears that the pressure dependence observed by Bawn and Evans may have been an artifact of their experimental diffusion flame technique. No curvature was observed in our lower pressure $P \leq 8$ torr conditions of this study and under these conditions, the recombination reaction appears to be in its low pressure, third order, limit.

In this limit, the recombination rate constant can best be calculated using unimolecular rate theory,[34] in which second-order rate constants for unimolecular decomposition are related through the equilibrium constant to the third order (low pressure) association rate constants. The unimolecular rate

constants are obtained using simplified equations of Troe based on RRKM theory.[35-36] The recombination rate constant can be expressed as the product of a strong collision rate constant $k^{sc}_{rec,o}$ and a weak collision deactivation efficiency term β_c,

$$k_{rec} = k^{sc}_{rec,o} \beta_c \tag{6}$$

In effect, β_c is a term expressing the efficiency by which $(NaO_2)^*$ is stabilized upon collision. In the absence of detailed state-to-state energy transfer rates, β_c is an adjustable parameter which depends on the average change in internal energy of the transition state complex per collision, $\langle\Delta E\rangle$, so that

$$\frac{\beta_c}{1-\beta_c^{1/2}} = \frac{\langle\Delta E\rangle}{F_E RT} \quad . \tag{7}$$

F_E is a correction term for the energy dependence of the density of states in the transition complex. Using a value of 163 kJ mole^{-1} for the Na-O_2 bond energy,[25] Patrick and Golden[37] have calculated k^{sc}_{rec} for Na + O_2 + (He) at 300 and 700 K. The computations result in $k^{sc}_{rec,o}$ (300 K) = 7.8 x 10^{-30} cm^6 s^{-1} for M = He. Thus, a value of β_c = 0.18 is required to reproduce the experimental result. The average energy transferred per collision is 0.8 kJ mole^{-1}. At 700 K, $k^{sc}_{rec,o}$ = 4.2 x 10^{-30} cm^6 s^{-1}, suggesting a value of β_c = 0.09 if $\langle\Delta E\rangle$ is assumed to be independent of temperature. Extrapolation of the experimental value for helium to 700 K results in an observed β_c = 0.14, in good agreement, considering the simplified assumptions of this approach.

This unimolecular approach has been shown to be fairly reliable in calculating termolecular association rate constants for a variety of species.[34,36] The values of β_c for M = N_2 and Ar tend to lie in the range of 0.1 - 0.5. The calculations for Na + O_2 in helium agree quite well with

these numbers, given that one might expect helium to be somewhat less efficient than N_2 in quenching the excited intermediate. For the similar reaction $H + O_2 + (N_2)$, the calculations also perform well, giving β_c = 0.08, even though the rate constant for this reaction, 5.9×10^{-32} cm^6 s^{-1} at 300 K,[38] is approximately 30 times slower than the corresponding sodium reaction.

In extrapolating our measured rate constants to higher pressures, it is important to understand the fall-off behavior as the reaction mechanism goes from its low pressure third order limit to its high pressure second order limit. A method for calculating the fall-off parameter based on RRKM theory has been developed by Luther and Troe.[39] Using their approach, the bimolecular rate constant in the transition region may be calculated as[34,38]

$$k^{II} = \frac{k_\infty k_o[M]}{k_\infty + k_o[M]} F^{\{1+[\log_{10}(k_o[M]/k_\infty)]^2\}^{-1}} \quad (8)$$

where k_∞ and k_o are the high pressure and low pressure limiting rate constants, respectively. The broadening parameter, F, is dependent on the molecular structure of the adduct and typically is on the order of 0.6 for small molecules.[34] The Patrick and Golden calculation for NaO_2^* gives F = 0.5.[37]

In order to assess the fall-off behavior, the association rate k_∞ may be estimated from the dynamics of the $Na + O_2$ encounter. Alkali atom reactions are often described in terms of their ionic character which leads to very fast reaction rates via an electron jump mechanism.[40] Ionic forces in the alkali-oxygen associations, however, are not as dominant as in other alkali atom reaction mechanisms. Although the approaching species do adiabatically transfer from the incident covalent potential surface to an ionic surface (electron jump mechanism), the crossing distance (r_c) is relatively small as compared with alkali-halogen systems and the overall association rate is dominated by the dispersion interaction on the covalent potential surface.

This is illustrated by comparing the rate constant based on the product of the mean collision velocity and the electron jump cross section (modified to account for the dispersion and angular momentum terms in the covalent potential function),[41] to a rate constant computed solely from a close collision model,[42] in which all collisions surmounting the angular momentum barrier of a Cr^{-6} potential contribute to the rate. For Na + O_2 at 300 K, an electron jump rate constant (r_c = 2.6 Å) is 1.5 x 10^{-10} cm^3 s^{-1}, while the close collision constant is 5.9 x 10^{-10} cm^3 s^{-1}. Thus, it appears that the rate of intermediate complex formation for reaction (2) is governed by long range dispersion forces, as found in most covalent systems. Once formed, however, these intermediates are certainly (alkali)$^+O_2^-$ ion pairs.[22] In either case, the association rate constant is expected to be fast with a value for $k_\infty > 10^{-10}$ cm^3 s^{-1}.

Using a value for $k_\infty = 2 \times 10^{-10}$ cm^3 s^{-1}, Eq. (8) may be used to estimate the ratio of the observed rate constant, k_{obs}, to the true third order low pressure limit, k_o. At the maximum density in our studies, 1.6 x 10^{17} cm^{-3}, one obtains $k_{obs}/k_o = 0.93$ which indicates that our experiments are essentially in the low pressure limit. For the conditions of Husain and Plane[28] (150 torr, 724 K), this same calculation would predict k_{obs}/k_o = 0.87. For the combustion conditions with P = 760 torr T = 2000 K applicable to the Hynes et al. study,[25] one obtains $k_{obs}/k_o = 0.89$. Thus, the large value for k_∞ would indicate that both of these studies are also essentially in the low pressure limit with regard to the recombination reaction.

Acknowledgements

The authors would like to thank Dr. F. Kaufman for many helpful discussions, and Drs. D. Golden and R. Patrick for performing association rate calculations for sodium. The technical assistance of W. Goodwin is greatly appreciated. This work was supported by the Air Force Geophysics Laboratory

under Contract Number F19628-83-C-0010, by the Army Research Office under Contract Number DAAG29-81-C-0024, and by the Chemical Manufacturers Association under Contract Number FC82-401.

REFERENCES

1. Friedman, R. and Levy, J.B.: Comb. Flame 7, 195 (1963)

2. Wolfhard, H.G., Glossman, I. and Green, L., Jr.: Prog. in Aeronautics and Astronautics 15, 419, Academic Press, 1964.

3. McHale, E.T.: Comb. Flame 24, 277 (1975)

4. Yousefian, V., May, I.W. and Heimerl, J.M.: "An Algebraic Criterion for the Prediction of Secondary Muzzle Flash - A Progress Report", 18th JANNAF Combustion Meeting, CPIA Publication 347, Vol. II, 63, Jet Propulsion Laboratory, Pasadena, CA, October, 1981.

5. Jensen, D.E. and Jones, G.A.: Comb. Flame 41, 71 (1981)

6. Reid, W.T.: External Corrosion and Deposits, Elsevier, New York, 1971.

7. Elston, C., Essenhigh, R.H., Cohn, A., and Stewart, G.W.: Coal Fired Gas Turbine Workshop Report, Electric Power Research Institute, Palo Alto, CA (1984).

8. Stearns, C.A., Kohl, F.J., and Rosner, D.E.: Proceedings of the NACE International Conference on High Temperature Corrosion, San Diego, CA (March, 1981).

9. Liu, S.C. and Reid, G.C.: Geophys. Res. Lett. 6, 283, (1979).

10. Kolb, C.E. and Elgin, J.B.: Nature 263, 488 (1976).

11. Chapman, S.: Astrophys. J. 90, 309 (1939).

12. Sze, N.D., Ko, M.C.W., Swider, W. and Murad, E.: Geophys. Res. Lett. 9, 1187 (1982).

13. Murad, E., Swider, W., and Bensen, S.W.: Nature 289, 273 (1981).

14. Silver, J.A., Stanton, A.C., Zahniser, M.S., and Kolb, C.E.: J. Phys. Chem. (accepted for publication, 1984).

15. Haber, F. and Sachsse, H.: Z. Physik. Chem. Bodenstein-Festband, 831 (1931)

16. Bawn, C.E.H. and Evans, A.G.: Trans. Faraday Soc. 33, 580 (1937)

17. Kaskan, W.E., Tenth Symposium (International) on Combustion, p. 41, The Combustion Institute, 1965.

18. Carabetta, R. and Kaskan, W.E.: J. Phys. Chem. 72, 2483 (1962).

19. McEwan, M.J. and Phillips, L.F.: Trans. Faraday Soc. 62, 1717 (1966).

20. Dougherty, G.J., McEwan, M.J. and Phillips, L.F.: Comb. Flame 21, 253 (1973).

21. Herm, R.R. and Hershbach, D.R.: J. Chem. Phys. 52, 5783 (1970)

22. Alexander, M.H.: J. Chem. Phys. 69, 3502 (1978).

23. Figger, H., Schrepp, W., and Zhu, X.: J. Chem. Phys. 79, 1320 (1983).

24. Jensen, D.E.: J. Chem. Soc. Faraday Trans. I 78, 2835 (1982).

25. Hynes, A.J., Steinberg, M. and Schofield, K.: J. Chem. Phys. 80, 2585 (1984).

26. Kramer, S.D., Lehmann, B.E., Hurst, G.S., Payne, M.G., and Young, J.P.: J. Chem. Phys. 76, 3614 (1982).

27. Grossman, L.W., Hurst, G.S., Kramer, S.D., Payne, M.G., and Young, J.P.: Chem. Phys. Lett. 50, 207 (1977).

28. Husain, D. and Plane, J.M.C.: J. Chem. Soc. Faraday Trans. II, 78, 163 (1982).

29. Husain, D. and Plane, J.M.C.: J. Chem. Soc. Faraday Trans. II, 78, 1175 (1982).

30. Gersh, M.E., Silver, J.A., Zahniser, M.S., Kolb, C.E., Brown, R.G., Gozewski, C.M., Kallelis, S. and Wormhoudt, J.C.: Rev. Sci. Inst. 52, 1213 (1981).

31. Brown, R.L.: J. Res. NBS 83, 1 (1978).

32. Silver, J.A.: "Diffusion Coefficients for Gaseous Alkali Species in Helium and Nitrogen" (submitted for publication, 1984).

33. Ferguson, E.E., Fehsenfeld, F.C. and Schmeltekopf, A.L.: Adv. Atomic Mol. Phys. 5, 1 (1969).

34. Patrick, R. and Golden, D.M.: Int. J. Chem. Kin. 15, 1189 (1983).

35. Troe, J.: J. Chem. Phys. 66, 4745 (1977).

36. Troe, J.: J. Chem. Phys. 66, 4758 (1977).

37. Patrick, R. and Golden, D.M., SRI International, private communication.

38. Baulch, D.L., Cox, R.A., Hampson, Jr., R.F., Kerr, J.A., Troe, J., and Watson, R.T.: J. Chem. Phys. Ref. Data 9, 295 (1980).

39. Luther, K. and Troe, J.: Seventeenth Symposium (International) on Combustion, p. 535, The Combustion Institute, 1979.

40. Levine, R.D. and Bernstein, R.B.: Molecular Reaction Dynamics, Oxford Press, 1974.

41. Gislason, E.A., Alkali Halide Vapors (P. Davidovits and D.L. McFadden, Ed.), Chap. 13, p. 415, Academic Press, 1979.

42. Johnston, H.S.: Gas Phase Reaction Rate Theory, p. 144 and 253, Ronald Press, 1966.

FIGURE CAPTIONS

Figure 1. Schematic view of the high temperature flow reactor.

Figure 2. Pseudo-first order decay of Na fluorescence signal vs. reaction distance for M = He at 309 K and 5.05 torr. $[O_2]$ = 1.09 (a), 3.36 (b), 7.29 (c), 14.3 (d), 26.6 (e); units of 10^{14} cm^{-3}. The estimated relative standard deviations for these points range from 1% to 4%.

Figure 3. Plots of first-order Na decay rates vs. $[O_2]$ for M = He and T = 309-335 K. Total pressure (torr) = 1.05 (o), 1.51 (•), 2.52 (+), 3.04 (Δ), 5.05 (∇). Each point has been corrected for the effects of diffusion and wall loss. Error bars correspond to $\pm 2\sigma$.

Figure 4. Plot of ln k(T) vs. ln T for the reaction Na + O_2 + M, with M = N_2 (circles), He (triangles), and Ar (square) for this work. The solid lines are least-square fits to these data. The + and x symbols represent data for M = N_2 and He, respectively from reference 28, and the dashed line (M = flame gases) is from reference 25.

Figure 5. Plot of ln k(T) vs. ln T for the reaction K + O_2 + M, with M = N_2 (circles), He (triangles), and Ar (square). The solid lines are least-square fits to these data. The + and x symbols represent data for M = N_2 and He, respectively from reference 29.

Table I. Comparison of Measured Rate Constants for $Na + O_2 + M \rightarrow NaO_2 + M$ and $K + O_2 + M \rightarrow KO_2 + M$

Reference	Alkali	Method	M	P (torr)	T(K)	k ($cm^6\ s^{-1}$)
This work	Na	Fast Flow Reactor Laser Induced Fluorescence	N_2	0.8-8.0	320-700	$(1.9 \pm 0.4) \times 10^{-30}\ (T/300)^{-1.1 \pm 0.5}$
			He	1.0-8.1	310-470	$(1.4 \pm 0.3) \times 10^{-30}\ (T/300)^{-0.9 \pm 0.5}$
			Ar	1.0-3.0	324	$(1.2 \pm 0.3) \times 10^{-30}$
Husain and Plane[28]	Na	Flash Photolysis Resonance Absorption	N_2	25-150	724	1.1×10^{-30}
					844	1.0×10^{-30}
			He	30-120	724	0.53×10^{-30}
					844	0.67×10^{-30}
Hynes et al.[25]	Na	Flame Studies with Laser Induced Fluorescence	$H_2O/O_2/N_2$ Mixtures	760	1650-2400	$2 \times 10^{-28}\ T^{-1}$
Bawn and Evans[16]	Na	Diffusion Flame	N_2	4-25	533	4.6×10^{-30}
This work	K	Fast Flow Reactor Laser Induced Fluorescence	N_2	1.0-6.0	302-720	$(5.4 \pm 0.2) \times 10^{-30}\ (T/300)^{-0.56 \pm 0.20}$
			He	1.0-6.0	296-520	$(2.0 \pm 0.5) \times 10^{-30}\ (T/300)^{-0.9 \pm 0.5}$
			Ar	1.6	300	$(3.5 \pm 1.0) \times 10^{-30}$
Husain and Plane[29]	K	Flash Photolysis Resonance Absorption	N_2	40-160	753	2.9×10^{-30}
					873	1.4×10^{-30}
			He	40-160	753	1.5×10^{-30}
					873	0.96×10^{-30}

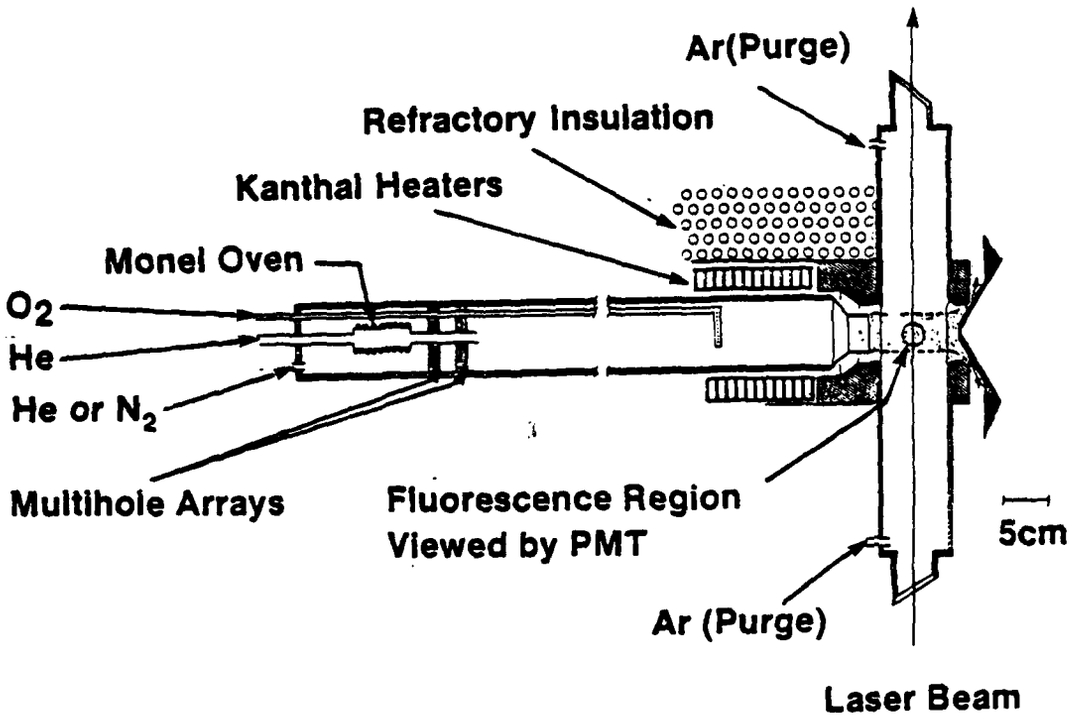
Ar(Purge)
Refractory Insulation
Kanthal Heaters
Monel Oven
O_2
He
He or N_2
Multihole Arrays
Fluorescence Region
Viewed by PMT
5cm
Ar (Purge)
Laser Beam

Figure 1

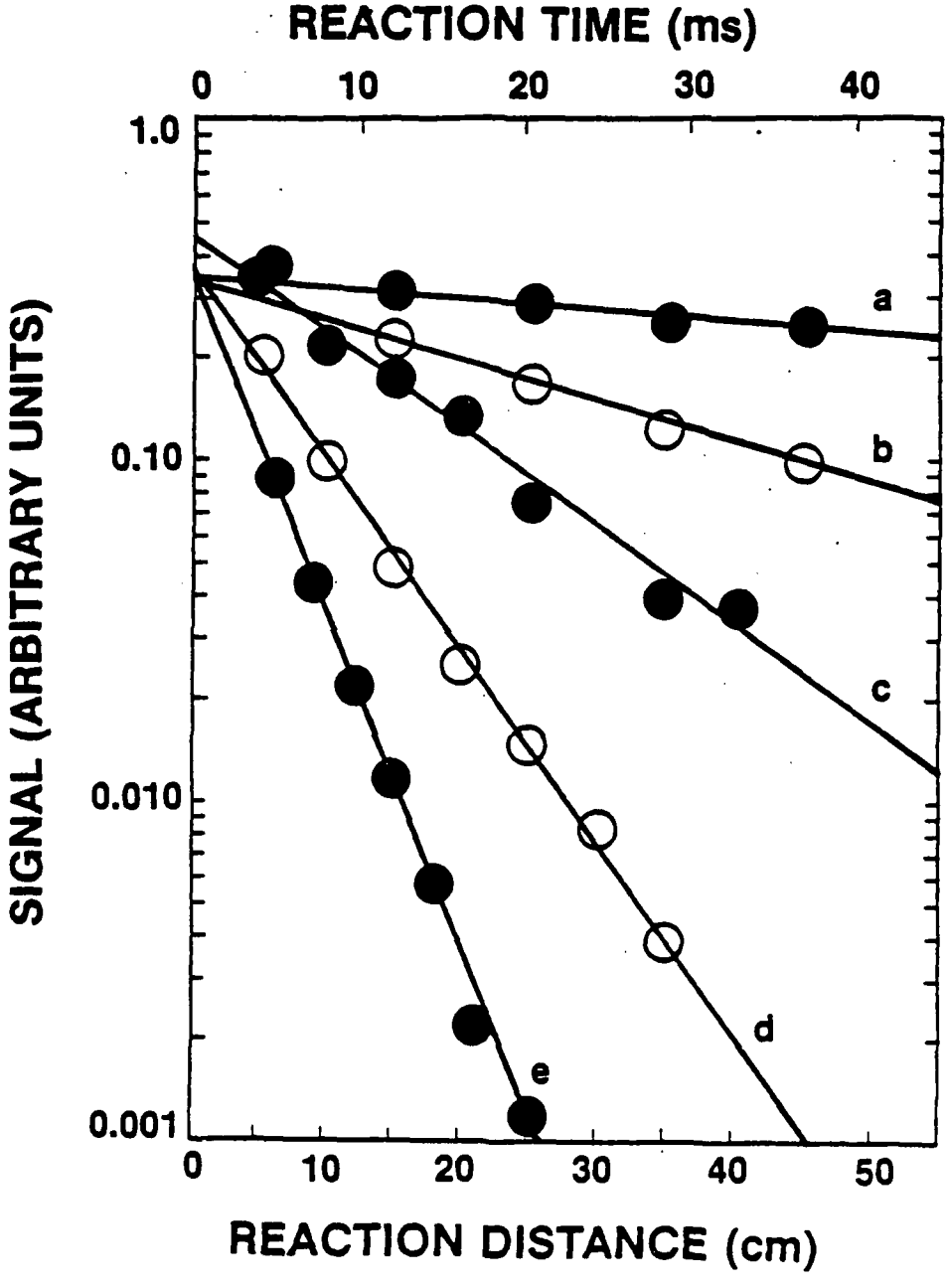
REACTION TIME (ms)
0
10
20
30
40
1.0
0.10
0.010
0.001
SIGNAL (ARBITRARY UNITS)
a
b
c
d
e
0
10
20
30
40
50
REACTION DISTANCE (cm)

Figure 2

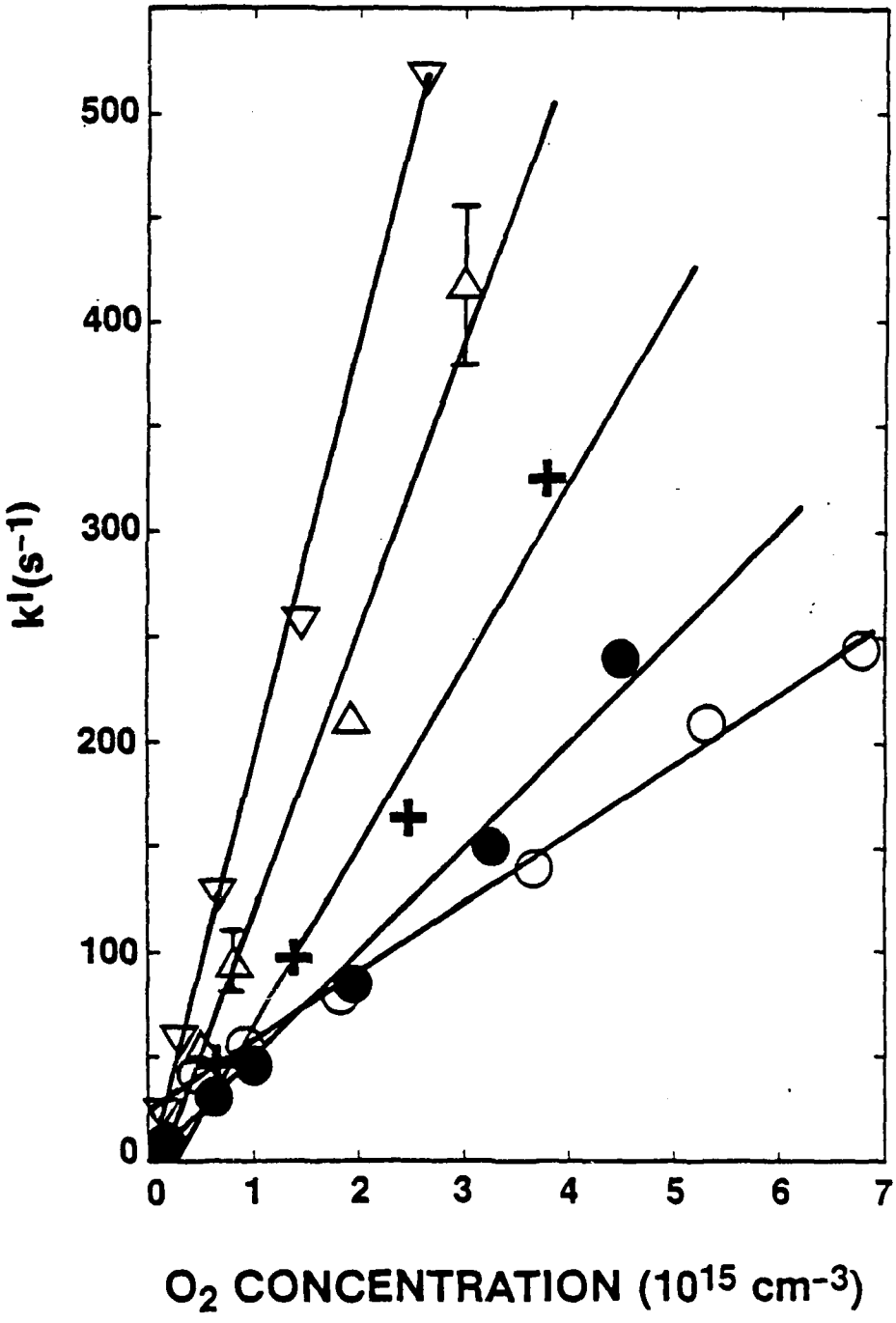
500
400
300
200
100
0
$k^1(s^{-1})$
0
1
2
3
4
5
6
7
O_2 CONCENTRATION (10^{15} cm^{-3})

Figure 3

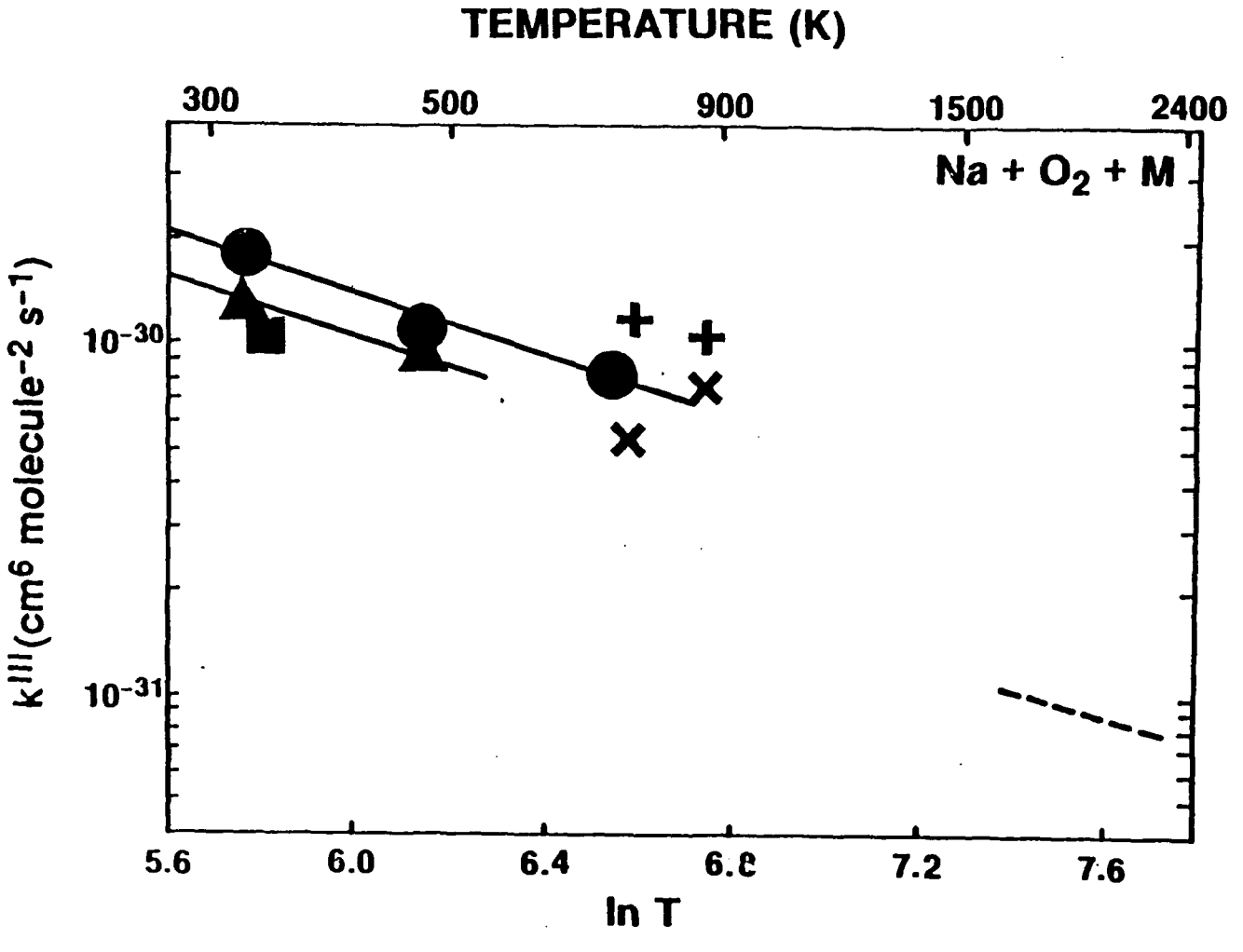
TEMPERATURE (K)
300
500
900
1500
2400
Na + O2 + M
10-30
10-31
k III (cm6 molecule-2 s-1)
5.6
6.0
6.4
6.8
7.2
7.6
ln T

Figure 4

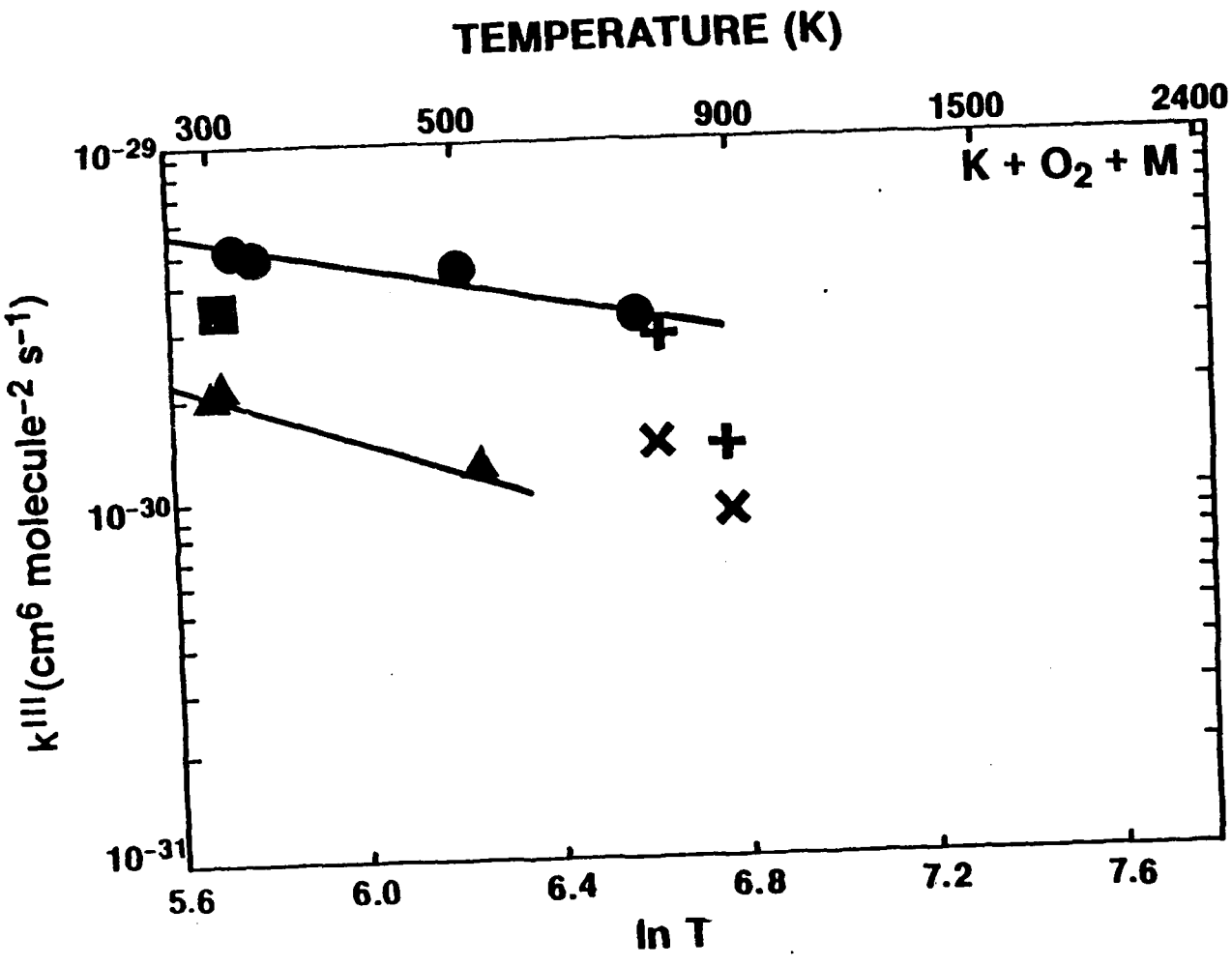
TEMPERATURE (K)
300
500
900
1500
2400
10^{-29}
10^{-30}
10^{-31}
$K + O_2 + M$
$k^{III}(cm^6\ molecule^{-2}\ s^{-1})$
5.6
6.0
6.4
6.8
7.2
7.6
ln T

Figure 5

APPENDIX B

THE GAS PHASE REACTION RATE OF SODIUM HYDROXIDE WITH HYDROCHLORIC ACID

Reprinted from The Journal of Physical Chemistry, 1984, 88, 3123.

Gas-Phase Reaction Rate of Sodium Hydroxide with Hydrochloric Acid

J. A. Silver,* A. C. Stanton, M. S. Zahniser, and C. E. Kolb

Center for Chemical and Environmental Physics, Aerodyne Research, Inc., Billerica, Massachusetts 01821
(Received: February 7, 1984)

The reactions of metallic species introduced into the atmosphere by meteor ablation may play a significant role in stratospheric chemistry. In particular, it has been suggested that the reaction of NaOH with HCl might affect the concentration of odd chlorine, thus having an impact on the ozone balance. This paper describes the first measurement of this reaction rate constant. At 308 K, we find that $k = (2.8 \pm 0.9) \times 10^{-10}$ cm^3 molecule^{-1} s^{-1}. As a result of the methods developed to perform this measurement, we have also determined estimates of the following room temperature rate constants in units of cm^3 molecule^{-1} s^{-1}: $k(\mathrm{NaO + HCl \rightarrow NaCl + OH}) \simeq 2.8 \times 10^{-10}$, $k(\mathrm{NaOH + H \rightarrow Na + H_2O}) > 4 \times 10^{-12}$, $k(\mathrm{NaCl + H \rightarrow Na + HCl}) \simeq 5 \times 10^{-(14\pm1)}$, and $k(\mathrm{Na + H_2O_2}) \simeq 6.9 \times 10^{-11}$, where approximately 0.6 of the reactions produce NaOH + OH, with the remainder forming NaO + H_2O.

Introduction

Metallic elements volatilized during meteor entry into the Earth's upper atmosphere play a significant role in the structure of the D and E regions of the ionosphere,[1-2] and, at least in the case of sodium, the visible day and nightglow emissions from the mesosphere and lower thermosphere.[3-5] Recently, it was suggested

(1) E. Murad, *J. Geophys. Res.*, 83, 5525 (1978).

(2) T. L. Brown, *Chem. Rev.*, 73, 645 (1973).
(3) J. E. Blamont and T. M. Donahue, *J. Geophys. Res.*, 69, 4093 (1964).
(4) D. M. Hunten, *Space Sci. Rev.*, 6, 493 (1967).

0022-3654/84/2088-3123$01.50/0

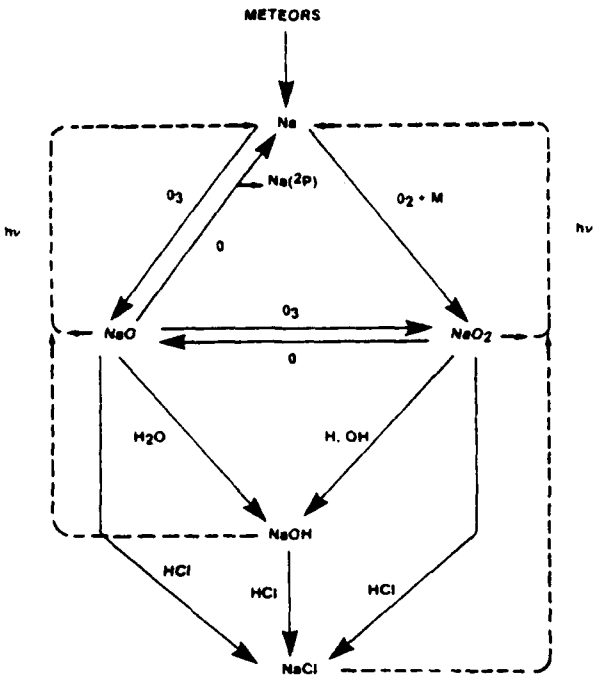

Figure 1. Schematic diagram of atmospheric sodium chemistry

that sodium and other meteor metals may be important in stratospheric chemistry by affecting ozone reduction by the catalytic chlorine cycle.[6-8]

The influx of meteor metals into the upper atmosphere has been estimated[9] to be 3.5×10^6 kg yr^{-1}, with a sodium abundance of 2% leading to a calculated sodium flux of 1.2×10^4 atoms cm^{-2} s^{-1}. Other estimates of sodium flux run as high as 2×10^4 cm^{-2} s^{-1}.[10] The flux of other metallic species such as Mg, Ca, Al, Si, and Fe will be as much as 10 times higher and speculative concerns about their influence on upper atmospheric homogeneous and heterogeneous chemistry have been published.[1-2,7-8,10]

Unfortunately, all attempts to model the role of volatilized meteor metals (particularly sodium) in the mesosphere and stratosphere[3-4,7,9-15] have suffered from an almost total lack of measured rate constants. All such models start with the oxidation of sodium or other metallic species in reaction with atmospheric O, O_2, or O_3. However, the only measured chemical rate constants currently available for any alkali meteor metal oxidation reactions are those for the three-body recombination reactions of alkali atoms (Na, K) with O_2[16-18]

$$\text{Na or K} + O_2 + M \rightarrow NaO_2 \text{ or } KO_2 + M \qquad (1)$$

In fact, until 2 years ago, even this reaction was thought to be ~1000 times slower[19-20] than the value found in the more recent measurements.

From the recent modeling work[7-8,10,13,21-22] and comparison of these models with atmospheric measurements,[12,14-15] neutral sodium is believed to be transformed via a series of chemical reactions involving NaO and NaO_2 intermediates to NaOH. A survey of the relevant literature[6-8,10,13] provides a fairly complete list of possible neutral sodium reactions of importance, and a simplified schematic diagram of these reactions is shown in Figure 1.

Neutral sodium appears in a range between 110- and 70-km altitude. As shown in Figure 1, the main removal mechanisms are by reaction with O_2 or O_3, the latter used by Chapman[23] to explain the Na nightglow. We have recently completed temperature-dependent measurements of the reaction rates with O_2 in our laboratory which show that this reaction proceeds with a fast three-body rate constant of 1.9×10^{-30} cm^6 s^{-1} with N_2 as the third body at 300 K.[18] This leads us to believe that most of the Na in the lower mesosphere is converted to NaO_2, since the three-body recombination rate with O_2 exceeds even a gas kinetic two-body rate with O_3 below 80 km. Since none of the remaining rates have ever been measured, the rest of the mechanism (as proposed by various models) is speculative. However, the dominant sodium species which leave the mesosphere and enter the stratosphere are probably NaOH and/or NaO_2.

The fate of NaOH is very uncertain. Indeed, only in the past few years has NaOH been recognized as a major reaction product. Ferguson[6] suggested that it forms NaOH cluster ions of the form $H^+(NaOH)_n(H_2O)_m$, which either may be rained out from the troposphere or removed in the stratospheric aerosol layer. In a recent paper by Murad et al.,[8] it was proposed that the reactions of metal hydroxides (and superoxides) with chlorine compounds between 40 and 70 km may have an impact on the depletion of stratospheric ozone. In the case of sodium, the exothermic bimolecular reactions

$$\text{NaOH} + \text{HCl} \rightarrow \text{NaCl} + H_2O \qquad \Delta H^\circ_r = -133 \pm 13 \text{ kJ mol}^{-1} \qquad (2)$$

$$\text{NaOH} + \text{ClO} \rightarrow \text{NaCl} + HO_2 \qquad \Delta H^\circ_r = -63 \pm 15 \text{ kJ mol}^{-1} \qquad (3)$$

$$\text{NaOH} + \text{Cl} \rightarrow \text{NaCl} + \text{OH} \qquad \Delta H^\circ_r = -67 \pm 13 \text{ kJ mol}^{-1} \qquad (4)$$

might be expected to proceed rapidly and act as a sink for Cl, given that NaCl can readily polymerize and condense via heterogeneous nucleation.[8] Murad et al. calculated that if k_2 were ~10^{-11} cm^3 molecule^{-1} s^{-1}, then the reaction of NaOH with HCl would be comparable to the major recognized Cl regeneration mechanism

$$\text{OH} + \text{HCl} \rightarrow \text{Cl} + H_2O \qquad (5)$$

While previously published studies have viewed NaCl as a potential sink for stratospheric chlorine,[7-8] more recent analyses by Rowland[24] indicate that photolysis of NaCl may in fact release free Cl. Given the potentially large J values (photolysis rates) for this process,[24] reactions 2–4 could effectively supplement reaction 5 as a release mechanism for Cl from the inactive HCl stratospheric reservoir and thereby determine the extent to which ozone might be depleted by chlorine compounds in the stratosphere. However,

(5) (a) V. W. J. H. Kirchhoff, B. R. Clemesha, and D. M. Simonich, *J. Geophys. Res.*, **84**, 1323 (1979); (b) D. R. Bates and P. C. Ojha, *Nature (London)*, **286**, 790 (1980).
(6) E. E. Ferguson, *Geophys. Res. Lett.*, **5**, 1035 (1978).
(7) E. Murad and W. Swider, *Geophys. Res. Lett.*, **6**, 929 (1979).
(8) E. Murad, W. Swider, and S. W. Benson, *Nature (London)*, **289**, 273 (1981).
(9) E. S. Richter and C. F. Sechrist, *Jr., J. Atmos. and Terr. Phys.*, **41**, 579 (1979); *Geophys. Res. Lett.*, **6**, 183 (1979).
(10) S. C. Liu and G. C. Reid, *Geophys. Res. Lett.*, **6**, 283 (1979).
(11) (a) W. J. Baggaley, *Nature (London)*, **257**, 567 (1975); (b) *ibid.*, **297**, 376 (1977); (c) M. A. Hapgood, *ibid.*, **286**, 582 (1980).
(12) V. W. J. H. Kirchhoff, B. R. Clemesha, and D. M. Simonich, *J. Geophys. Res.*, **86**, 6892 (1981).
(13) N. D. Sze, M. K. W. Ko, W. Swider, and E. Murad, *Geophys. Res. Lett.*, **9**, 1187 (1982).
(14) V. W. J. H. Kirchhoff, *Geophys. Res. Lett.*, **10**, 721 (1983).
(15) L. Thomas, M. C. Isherwood, and M. R. Bowman, *J. Atmos. Terr. Phys.*, **45**, 587 (1983).
(16) D. Husain and J. M. C. Plane, *J. Chem. Soc., Faraday Trans. 2*, **78**, 163, 1175 (1982).
(17) A. J. Hynes, M. Steinberg, and K. Schofield, *J. Chem. Phys.*, **80**, 2585 (1984).
(18) J. A. Silver, M. S. Zahniser, A. C. Stanton, and C. E. Kolb, *Symp. (Int.) Combust. [Proc.], 20th*, accepted for publication.
(19) R. Carabetta and W. E. Kaskan, *J. Phys. Chem.*, **72**, 2483 (1968).
(20) M. J. McEwan and L. F. Phillips, *Trans. Faraday Soc.*, **62**, 717 (1966).
(21) C. E. Kolb and J. B. Elgin, *Nature (London)*, **263**, 488 (1976).
(22) D. M. Simonich, B. R. Clemesha, and V. W. J. H. Kirchhoff, *J. Geophys. Res.*, **84**, 1543 (1979).
(23) S. Chapman, *Astrophys. J.*, **90**, 309 (1939).
(24) F. S. Rowland and P. J. Rogers, *Proc. Natl. Acad. Sci. U.S.A.*, **79**, 2737 (1982).

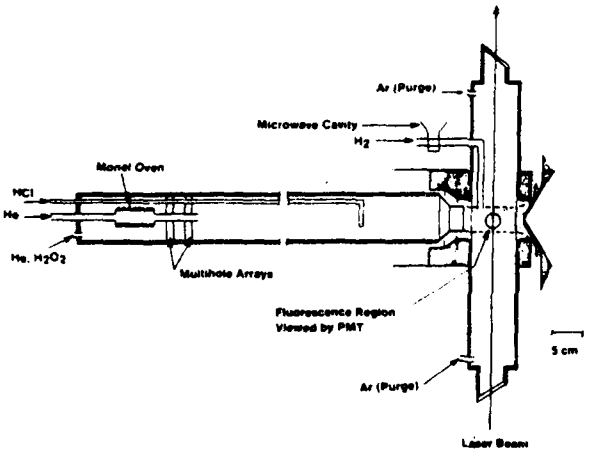

Figure 2. Schematic view of the flow tube

to understand fully the role of alkali species in the atmosphere, one must also consider the effects of NaO_2 and NaOH photodissociation on these processes.[13,25]

The purpose of this study is to provide a direct experimental rate measurement of the reaction $NaOH + HCl \rightarrow NaCl + H_2O$, which serves as a starting point for understanding the stratospheric role of sodium and other meteor metals. Only by obtaining accurate, directly measured rate constants can we hope to understand atmospheric metal chemistry, and, in particular, how this chemistry affects the ozone balance.

Experimental Section

Very little gas-phase research has been done on alkali hydroxides because they are difficult to vaporize,[26] are extremely corrosive,[27] and readily dimerize in the gas phase.[28] In addition, there are no established detection techniques sensitive enough to allow kinetic analyses of alkali hydroxide reactions. With this in mind we have taken an indirect approach for producing and detecting NaOH, i.e., chemical production of NaOH by the reaction of atomic sodium with hydrogen peroxide, and detection of NaOH by chemical conversion back to atomic sodium, which is then observed by laser-induced fluorescence.

The measurements were performed in the Aerodyne high-temperature fast-flow reactor, which is fully described in ref 29 and whose relevant features are illustrated in Figure 2. Briefly, a 7.26-cm-diameter, 120-cm-long alumina tube is used, fitted with Kanthal heater elements which can radiatively heat the tube over the temperature range 294–1500 K. Four perpendicular alumina side arms at the tube exit permit detection of flow species by a variety of optical techniques, including laser- or resonance lamp-excited fluorescence, infrared absorption (either broad band or high resolution), and observation of chemiluminescence. Gas temperatures are obtained with chromel–alumel or shielded W–5% Re—W–26% Re thermocouples.[30] Extensive calibrations indicate the temperature can be measured with an accuracy of ±10 K over the entire operating range of the reactor for flow Reynolds numbers below 500; for the current experiments they are typically below 50. The gas is pumped by a Kinney KMBD 1602 mechanical pump and Roots blower with an effective pumping speed of 450 L s^{-1}. The helium carrier gas is added at the entrance of the flow tube through mullite multichannel arrays which laminarize the flow. These are ~2.5-cm upstream of the outlet of the reactant inlet tube and 78 cm from the detection region. This allows sufficient distance (18 cm) for the helium flow to mix with the reactants and develop a parabolic velocity profile before reaching the reaction zone. Gas volumetric flow rates are determined with calibrated thermal conductivity type mass flow meters. Flow speeds can be varied from 4 to 100 m s^{-1}. A calibrated MKS Baratron Model 310-BSH10 capacitance manometer (0.8% accuracy) is used to measure pressure.

Alkali atoms are generated by heating the sample in a 2.5-cm-diameter cylindrical monel oven to a temperature commensurate with attaining a vapor pressure of that species of 10^{-6} to 10^{-4} torr within the oven. The oven is silver plated to resist alkali corrosion.[27] The vapor is entrained in a flow of inert carrier gas and introduced into the flow tube through a 10-cm section of 19-mm o.d. silver tubing. The sodium vapor is further diluted by the carrier gas in the main flow tube so that the sodium concentration within the reaction zone is always less than 10^{10} cm^{-3}. For wall removal rate measurements the entire oven assembly may be placed downstream of the mullite arrays as a movable source. Since the oven is heated, it warms the main carrier gas flow slightly. Axial temperature surveys in the reaction region show that the final flow temperature profile is uniform at a value of 308 K.

Sodium hydroxide is produced via the reaction

$$\begin{gathered} Na + H_2O_2 \rightarrow NaOH + OH \\ \Delta H^\circ_r = -130 \pm 13 \text{ kJ mol}^{-1} \end{gathered} \quad (6)$$

The H_2O_2 is added upstream of the mullite arrays with the main carrier gas. An all glass and teflon inlet system is used to prevent decomposition of H_2O_2 between its reservoir and the flow tube. Flow rates of H_2O_2 are determined by entraining the vapor in a measured helium flow at a known total reservoir pressure, where

$$H_2O_2 \text{ flow} = (P_{H_2O_2}/P_{total})(\text{He flow through system}) \quad (7)$$

The partial pressure of H_2O_2 at 25 °C is 2.0 torr.

Detection of NaOH is accomplished by converting it back to atomic sodium in the detection region, where the sodium is measured by laser-induced fluorescence (LIF). This conversion is accomplished by injecting an excess of atomic hydrogen into the flow 2-cm upstream of the LIF detector.

$$\begin{gathered} NaOH + H \rightarrow Na + H_2O \\ \Delta H^\circ_r = -154 \pm 13 \text{ kJ mol}^{-1} \end{gathered} \quad (8)$$

$$Na + h\nu \rightarrow Na^* \rightarrow Na + h\nu \qquad \text{LIF detection} \quad (9)$$

The hydrogen atoms, produced by microwave discharge of pure molecular hydrogen, are introduced through a teflon-lined 6-mm-diameter tube. With the mean flow velocity of 1000 cm s^{-1}, the reaction time of hydrogen in the detector (t_d) is 2 ms. The atomic hydrogen concentration is estimated to be 2×10^{14} cm^{-3}, by measuring the H_2 flow rate and assuming that 10% of the H_2 passing through the discharge dissociates,[31] with no recombination[32] or loss on the inlet tube walls.[31]

A Molectron DL14 nitrogen pumped dye laser is used for laser-induced fluorescence detection of Na. The laser-induced fluorescence data acquisition system and manipulation of data have been detailed elsewhere.[33] However, it should be noted that fluorescence is usually averaged over 100 laser pulses, accounting for nonfluorescent background signals and for pulse-to-pulse fluctuations in laser intensity. The combined signal-to-noise ratio for these measurements generally exceeds 25.

Purities of the chemicals used in these experiments are as follows: sodium metal, 99.95% (Alfa); helium, 99.995% (Northeast Cryogenics); hydrogen, 99.995% (Air Products); nitrogen, 99.998% (Northeast Cryogenics); and hydrogen chloride, 99.99% (Northeast Cryogenics). Hydrogen peroxide, obtained

(25) F. S. Rowland and Y. Makide, *Geophys. Res. Lett.*, **9**, 473 (1982).
(26) "JANAF Thermochemical Tables", The Dow Chemical Company, Midland, MI, 1970.
(27) N. Acquista and S. Abramowitz, *J. Chem. Phys.*, **51**, 2911 (1969).
(28) R. C. Schoonmaker and R. F. Porter, *J. Chem. Phys.*, **28**, 454 (1958).
(29) M. E. Gersh, J. A. Silver, M. S. Zahniser, C. E. Kolb, R. G. Brown, C. M. Gozewski, S. Kallelis, and J. C. Wormhoudt, *Rev. Sci. Instrum.*, **52**, 1213 (1981).
(30) A. Fontijn and W. Felder, *J. Phys. Chem.*, **83**, 24 (1979).
(31) W. E. Jones, S. D. MacKnight, and L. Teng, *Chem. Rev.*, **73**, 407 (1973).
(32) D. W. Trainor, D. O. Ham, and F. Kaufman, *J. Chem. Phys.*, **58**, 4599 (1973).
(33) J. A. Silver and C. E. Kolb, *J. Phys. Chem.*, **86**, 3240 (1982).

TABLE I: Typical Experimental Conditions

temp, K	308
flow velocity, m s^{-1}	10.0
press., torr	2.0
[Na], cm^{-3} (initial)	$\leq 10^{10}$
[H_2O_2], cm^{-3}	1.3×10^{13}
[HCl], cm^{-3}	$(1-4) \times 10^{12}$
[H], cm^{-3}	2×10^{14}

as a 90% (by weight) solution from FMC Corp., is purified by *vacuum distillation. Titration with potassium permanganate* indicates a resulting purity on the order of 99%. This corresponds to a purity in the vapor phase of ~93%, with the balance being water vapor.

Rate measurements are made with one reactant in excess of the other (detected) reactant, thus ensuring pseudo-first-order kinetic conditions. Reaction times are varied by changing the injector position at fixed total flow velocity and pressure. Corrections for both axial and radial diffusion and wall removal are made with the procedure outlined by Brown.[34] This method is based on a numerical solution of the equations describing diffusion and reaction in a flow tube. It assumes that Poiseuille flow exists and provides ranges for k, k_w (wall removal), and D (diffusion coefficient) for which the solutions have been shown to be valid. Wall removal rates of the measured species are determined in separate experiments by varying the oven position. The observed wall removal rate, as well as the reaction rate, is corrected for diffusion effects. Diffusion constants for alkali atoms and hydroxides were obtained from wall removal measurements in the instance where the observed disappearance of the species is diffusion limited.[35] At 308 K, D(Na–He) = 0.50 atm cm^2 s^{-1} and D(NaOH–He) = 0.47 atm cm^2 s^{-1}.

An important aspect of the data analysis is the ability to ensure that secondary reactions have no effect on the concentration of the species being monitored. This could dramatically affect the accuracy of the rate measurements. The effects of secondary reactions are determined by modeling the reactions occurring in the flow tube. This is done with the Aerodyne PACKAGE code,[36] a kinetic modeling program which numerically integrates the differential rate equations for a specified set of reactions. Backward reaction rates determined from the JANAF thermochemical tables and the forward rates are included, to ensure that accuracy is maintained.

Results

$Na + H_2O_2$ Reaction. The NaOH formation rate was measured by directly observing the disappearance of sodium, with H_2O_2 in known excess. The reaction has two exothermic product channels

$$\mathrm{Na + H_2O_2 \rightarrow NaOH + OH} \qquad \Delta H^\circ_r = -130 \pm 13 \text{ kJ mol}^{-1} \tag{6}$$

$$\mathrm{Na + H_2O_2 \rightarrow NaO + H_2O} \qquad \Delta H^\circ_r = -130 \pm 42 \text{ kJ mol}^{-1} \tag{6'}$$

so what is measured by monitoring Na disappearance is the total reaction rate. However, one can add excess CO (~2×10^{15} cm^{-3}), which rapidly and quantitatively converts NaO to Na[37-38]

$$\mathrm{NaO + CO \rightarrow Na(^2S) + CO_2} \qquad \Delta H^\circ_r = -259 \pm 42 \text{ kJ mol}^{-1} \tag{10}$$

$$\mathrm{NaO + CO \rightarrow Na(^2P) + CO_2} \qquad \Delta H^\circ_r = -56 \pm 42 \text{ kJ mol}^{-1} \tag{10'}$$

(34) R. L. Brown, *J. Res. Natl. Bur. Stand.*, 83, 1 (1978)
(35) J. A. Silver, manuscript in preparation.
(36) V. Yousefian, M. H. Weinberg, and R. Haimes, "PACKAGE: A Computer Program for Calculation of Partial Chemical Equilibrium/Partial Finite Chemical Rate Controlled Composition of Multiphased Mixtures Under One Dimensional Steady Flow", Aerodyne Research, Inc., Report No. ARI-RR-177, Feb 1980.
(37) C. P. Fenimore and J. R. Kelso, *J. Am. Chem. Soc.*, 72, 5045 (1950)
(38) R. C. Benson, C. B. Bargeron, and R. E. Walker, *Chem. Phys. Lett.*, 35, 161 (1975)

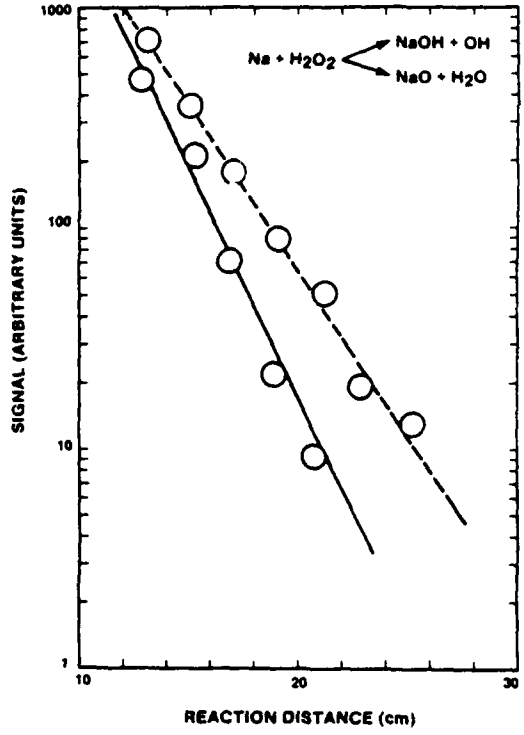

Figure 3. Pseudo-first-order decays for Na + H_2O_2 reaction. The solid line is the total reaction rate; the dashed line is the rate for branching to NaOH only (CO added).

Although the value for k_{10} has not been measured, indirect estimates from ref 37 imply $k_{10} \geq 10^{-11}$ cm^3 $molecule^{-1}$ s^{-1}. The large amount of CO added is required to ensure that all of the NaO cycles back to Na on a time scale much shorter than the time required for reaction 6 to occur.

A rate measurement with CO present results in the production rate for only the NaOH branch. The results of these measurements are shown in Figure 3. Experimental conditions are given in Table I. The rate constant for both channels is $k_{6+6'} = (6.9 \pm 3.0) \times 10^{-11}$ cm^3 $molecule^{-1}$ s^{-1}, and the fraction in the NaOH product channel is 0.61 ± 0.10. The major uncertainty in the rate constants k_6 and $k_{6'}$ is the H_2O_2 concentration, which is not directly measured but is obtained as indicated earlier.

An independent determination of the product branching ratio for reaction 6 is obtained by observing the hydroxyl radical via laser-induced fluorescence at 308.6 nm. When Na reacts with H_2O_2, only the NaOH product channel produces OH. However, when excess HCl is added to the NaO and NaOH product mixture, additional OH is formed by the reaction

$$\mathrm{NaO + HCl \rightarrow NaCl + OH} \qquad \Delta H^\circ_r = -134 \pm 42 \text{ kJ mol}^{-1} \tag{11}$$

Thus a measurement of the amounts of OH produced before and after addition of HCl provides the relative amounts of NaOH and NaO originally formed from Na + H_2O_2. The observed NaOH product fraction by this method is 0.60 ± 0.10, in excellent agreement with the value obtained from the rate measurements.

NaOH + HCl Reaction. In the presence of excess CO, the reaction of sodium with hydrogen peroxide produces only NaOH. With this reaction used as a source for NaOH, a series of rate measurements were made for the reaction of NaOH with HCl. First-order decays were linear for more than a factor of 10 in fluorescence signal, with the HCl concentrations ranging from 1×10^{12} to 4×10^{12} cm^{-3}. The results of these experiments are shown in Figure 4, and the rate constant for this reaction is $k_2 = (2.8 \pm 0.9) \times 10^{-10}$ cm^3 $molecule^{-1}$ s^{-1}. The uncertainty expressed includes estimated precision errors at a 95% confidence level, as well as estimated errors in accuracy.

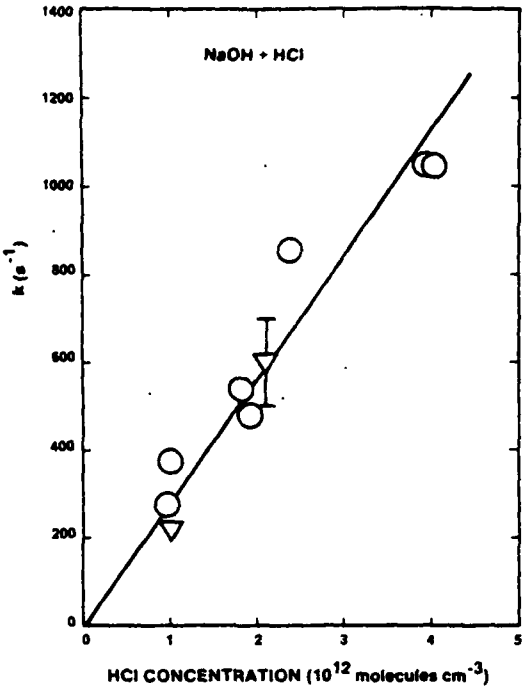

Figure 4. First-order reaction rates vs. [HCl] for the reactions of NaOH (NaO) + HCl: (○) without CO added; (▽) with CO added.

Separate measurements were also made without adding CO. In this case NaO, in addition to NaOH, is present and reacts with HCl (reaction 11), complicating the analysis. Furthermore, the detection scheme, based on conversion to Na by addition of atomic hydrogen, would not appear to distinguish between NaO and NaOH, since Na atoms are also produced in the reaction

$$\text{NaO} + \text{H} \rightarrow \text{Na} + \text{OH} \qquad \Delta H^\circ_r = -155 \pm 42 \text{ kJ mol}^{-1} \quad (12)$$

Thus, without CO, the decrease in signal upon addition of HCl is due to both reactions 2 and 11, weighted by the branching ratio from reaction 6,6'. The results, however, show the same decay with and without added CO (see Figure 4), implying that both NaO and NaOH react with HCl at approximately the same rate. This observation is reasonable if one considers the hydroxyl group on NaOH to act as a quasi-atom in respect to its chemical behavior given identical exothermicities for both reactions.

Separate OH measurements confirm that atomic hydrogen reacts with NaO as well as with pure NaOH. Although we could not measure the NaO + HCl rate constant directly, the observation that (1) OH is formed in the NaO + H reaction (proving the existence of NaO), (2) OH is also formed upon addition of HCl to NaO, and (3) the decay rates with added HCl are identical both with or without CO, imply that NaO reacts with HCl at approximately the same rate as NaOH with HCl.

Detector Corrections and Modeling. Although the plots of ln (signal) vs. reaction time are linear over the first order of magnitude decrease in signal, at longer times they flatten out at a value typically a few percent of the initial (zero reaction time) signal (Figure 5). This effect can be attributed to an additional component to the Na signal from the reaction

$$\text{NaCl} + \text{H} \rightarrow \text{Na} + \text{HCl} \qquad \Delta H^\circ_r = -21 \pm 2 \text{ kJ mol}^{-1} \quad (13)$$

For the case with CO present, sodium formed in the detection region by addition of atomic hydrogen has two sources, NaOH and NaCl, the amount of each depending on the extent to which the NaOH + HCl → NaCl + H_2O reaction has gone to completion. The rate equation for the formation of sodium in the detector is

$$d[\text{Na}]/dt = k_8[\text{NaOH}]_d[\text{H}] + k_{13}[\text{NaCl}]_d[\text{H}] \quad (14)$$

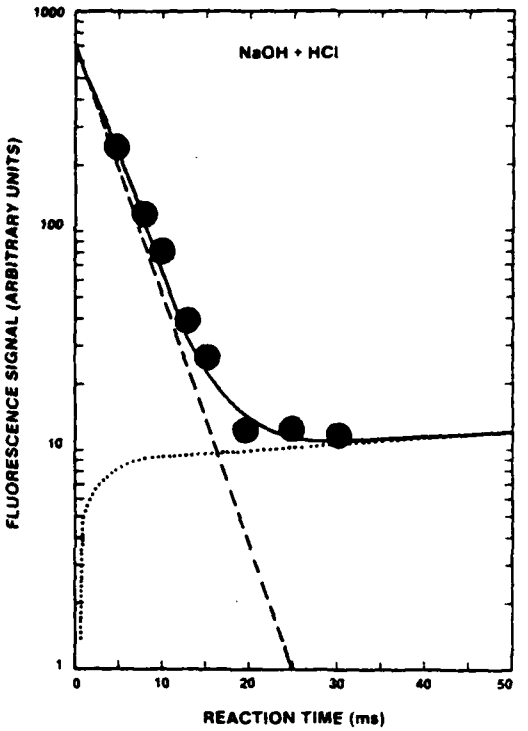

Figure 5. Typical decay of fluorescence signal vs. reaction time for NaOH + HCl, showing contribution to total detected sodium (—) from NaOH (– – –) and NaCl (····). Circles are experimental data.

where the d subscript indicates the concentration at the entrance to the detector zone. Integrating over the detector reaction time (t_d), assuming excess hydrogen, we obtain

$$[\text{Na}] = [\text{NaOH}]_d(1 - e^{-k_8[\text{H}]t_d}) + [\text{NaCl}]_d(1 - e^{-k_{13}[\text{H}]t_d}) \quad (15)$$

If no HCl is added, the observed LIF signal arises solely from NaOH. We have observed that this signal (after correcting for differences in diffusion and wall removal between Na and NaOH) is identical with that arising from only sodium (i.e., without H_2O_2 added). This means that, within the available detector reaction time, all of the NaOH is converted to sodium, with an estimated error of 20%. This sets a lower limit to $k_8[\text{H}]t_d$. Given $t_d = 2$ ms and $[\text{H}] \simeq 2 \times 10^{14}$ cm^{-3}, this requires that $k_8 \geq 4 \times 10^{-12}$ cm^3 molecule^{-1} s^{-1}. The accuracy of t_d is ±0.5 ms. If less than 10% of the H_2 is dissociated (it is unlikely to be higher under our operating conditions), then k_8 is faster than the stated limit.

This value for k_8 is in reasonable agreement with a value of $1 \times 10^{-12}T^{1/2}$ (1.7×10^{-11} cm^3 molecule^{-1} s^{-1} at 300 K) which is used by Hynes et al.[17] in fitting their flame data over a wide range of conditions, and also with $2 \times 10^{-11}e^{-800/T}$ (1.4×10^{-12} at 300 K), which is used in various atmospheric models.[10,13] The former value is claimed to be accurate to within a factor of two at flame temperatures, and the latter is only an estimate. We are planning to perform direct measurements of this reaction in the near future.

Now if we measure the reaction rate of NaOH + HCl, at short reaction times the decay in signal is logarithmic because $[\text{NaOH}]_d > [\text{NaCl}]_d$, and only the first term in eq 15 is significant. At long reaction times, $[\text{NaCl}]_d > [\text{NaOH}]_d$ and the second term becomes dominant (Figure 5). If $k_{13} = k_8$, we would never observe a decay in [Na] since both terms in eq 15 would always have the same sum. However, the fact that an initial decay is observed with a later leveling of signal shows that $k_{13} << k_8$ and, from the relative value of the signal where it levels off, we can estimate k_{13}.

To determine k_{13}, we modeled this reaction system using the conditions in Table II and rate set in Table III. This rate set is more extensive than the above discussion implies because there could be secondary reactions between the excess H_2O_2 and the sodium formed in the detector, as well as other minor OH, H,

TABLE II: Initial Conditions Used in Chemical Model

temp, K	308
flow velocity, m s^{-1}	10.0
press., torr	2.0
[Na], cm^{-3} (initial)	10^{10}
$[H_2O_2]$, cm^{-3}	1.3×10^{13}
[HCl], cm^{-3}	1.93×10^{12}
$[H]_d$, cm^{-3}	2×10^{13}–1×10^{15}
$[H_2]_d$, cm^{-3}	10^{15}–10^{16}
$[H_2O]$, cm^{-3}	7×10^{11}
t_{ma}, ms	0–25
t_d, ms	0.5–4.0

TABLE III: Reaction Rate Set Used for Modeling Na Chemistry[a]

reaction	k, cm^3 molecule^{-1} s^{-1}	ref
$Na + H_2O_2 \rightarrow NaOH + OH$	$6.9(-11)$	*b*
$NaOH + HCl \rightarrow NaCl + H_2O$	$2.8(-10)$	*b*
$NaOH + H \rightarrow Na + H_2O$	$1.0(-10)$–$1.0(-14)$	*b*
$NaCl + H \rightarrow Na + HCl$	$1.0(-10)$–$1.0(-14)$	*b*
$Na + HO_2 \rightarrow NaOH + O$	$1.0(-10)$	est
$2HO_2 \rightarrow H_2O_2 + O_2$	$1.6(-12)$	39
$O + H_2O_2 \rightarrow OH + HO_2$	$1.0(-11)e^{-2500/T}$	40
$OH + H_2O_2 \rightarrow H_2O + HO_2$	$2.96(-12)e^{-164/T}$	41
$H + H_2O_2 \rightarrow H_2 + HO_2$	$2.13(-12)e^{-1400/T}$	42
$H + H_2O_2 \rightarrow OH + H_2O$	$2.76(-12)e^{-1400/T}$	42
$H_2 + OH \rightarrow H + H_2O$	$7.7(-12)e^{-2100/T}$	40
$H_2 + O \rightarrow H + OH$	$1.6(-11)e^{-4570/T}$	40
$OH + HO_2 \rightarrow H_2O + O_2$	$8.0(-11)$	40
$H + HO_2 \rightarrow 2OH$	$3.2(-11)$	40
$H + HO_2 \rightarrow H_2 + O_2$	$1.4(-11)$	40
$H + HO_2 \rightarrow H_2O + O$	$9.4(-13)$	40
$O + HO_2 \rightarrow O_2 + OH$	$8.0(-11)e^{-500/T}$	40
$2OH \rightarrow O + H_2O$	$1.8(-12)$	40
$HCl + OH \rightarrow H_2O + Cl$	$6.6(-13)$	40

[a] No three-body rates were used because the system is at low pressure. [b] This work.

etc. reactions. This model also includes the undissociated hydrogen, and the water impurity (~7%) in the H_2O_2. We systematically varied k_8, k_{13}, [H], $[H_2O_2]$, and t_d. The results show that all secondary reactions have little effect (<5%) on the calculated sodium densities and that the variations of Na with $[H_2O_2]$ and $[H_2]$ are small, in reasonable agreement with additional experiments. The value for k_{13} which best fits the experimental data is $(8 \pm 3)/[H]$, which leads to value of k_{13} in the range 1×10^{-14} to 5×10^{-13} cm^3 $molecule^{-1}$ s^{-1}, with a best estimate of 5×10^{-14} cm^3 $molecule^{-1}$ s^{-1}. In light of the small exothermicity for this reaction, this value is not unreasonable. If the rate constant is expressed in the Arrhenius form, $k = Ae^{-E/RT}$, this would correspond to only a 21 kJ mol^{-1} barrier, even with a gas kinetic preexponential term.

Discussion

The reaction rate constant of HCl with NaOH is found to be in its gas kinetic limit. Given the large exothermicity, absence of obvious steric effects, and the fact that reactant and product states correlate on a singlet potential energy surface, one might not consider this surprising. On the other hand, the strong covalent HCl bond must be broken during the reaction with an efficiency approaching unity. One can calculate a rate constant for this reaction using simple close collision theory.[43] This procedure assumes that the attractive portion of the intermolecular potential varies as Cr^{-6}, where C depends on the dipole moments and static polarizabilities of the reactants,[44] and r is the intermolecular distance. The total effective potential energy curve at large r is this attractive portion plus a centrifugal term which accounts for orbital angular momentum. The rate of close collisions is identified as applying to collisions with total energy sufficient to surmount the orbital angular momentum barrier in this effective potential energy curve. If it is assumed that all close collisions react, and that there is no activation energy, the rate constant calculated for NaOH + HCl is 1.8×10^{-10} cm^3 $molecule^{-1}$ s^{-1}, in good agreement with the measured value.

Few gas-phase reactions of alkali molecules have been studied, none involving alkali hydroxides. The alkali–hydroxide bond is ionic in character, so that $(OH)^-$ is a closed-shell species, not dissimilar to its isoelectronic and isobaric analogue, F^-. Thus, in absence of data on NaOH, we can use available information on NaF and other alkali halides to try to understand the properties of the alkali hydroxides. There have been a number of molecular beam scattering measurements of alkali halides with other alkali halides or hydrogen halide molecules.[45] As a class, they all imply the existence of a strong collision complex. In the case of CsCl + KI → CsI + KCl, the reaction proceeds without any activation energy (despite being four-centered) and has a large total cross section.[46] This has been explained by the large ionic character of both species and by the fact that alkali halide dimers have large binding energies in the geometry of a cyclic planar rhomboid.[45] This ion-pair intermediate formulation has also been invoked in describing the BaI_2 + HCl reaction,[47] where, for large alkaline earths such as barium, we can treat BaI_2 as $(BaI)^+I^-$. What we can draw from these comparative systems is that a gas kinetic rate constant without any activation barrier is a reasonable expectation for this system. In the extrapolation of the measured rate data to lower temperatures characteristic of the stratosphere, one would not expect any great dependence on temperature for the reaction rate.

The importance of reaction 2 in stratospheric ozone chemistry may be estimated by comparing the Cl regeneration rates from HCl via reaction with OH with regeneration rates from reaction with NaOH followed by photolysis of NaCl. Estimates of stratospheric NaCl photolysis rates by Rowland and Rogers[24] are in the range from 10^{-2} to 10^{-3} s^{-1}. At 40 km, the meteoric sodium is partitioned among the species NaOH, NaO_2, and NaO. Estimates of total stratospheric sodium concentrations by Liu and Reed[10] are on the order of 5×10^5 cm^{-3}. If all of the meteoric sodium were in the form of NaOH at 40 km, our measurement of k_2 would give a first-order rate constant for Cl formation of 1.4×10^{-4} s^{-1}, providing that J_{NaCl} is in the range estimated by Rowland and Rogers. This is a factor of ~20 faster than the first-order rate constant for Cl regeneration from OH + HCl of 6×10^{-6} s^{-1}, based on an OH concentration of 10^7 cm^{-3} and the value $k_5(250\ K) = 5.7 \times 10^{-13}$ cm^3 $molecule^{-1}$ s^{-1}.[48] Although the partitioning of total sodium among NaOH, NaO, and NaO_2 requires a more detailed knowledge of rate constants for the processes shown in Figure 1, this calculation demonstrates that, even if only 5% is in the form of NaOH, regeneration of Cl from HCl via alkali chemistry would be comparable to regeneration by the OH reaction.

This simple computation leads us to two conclusions. First, our results for this and the other alkali reactions described show that meteoric metal reactions may have a potentially significant impact on our understanding of chemistry in the mesosphere and upper stratosphere. The large values of the sodium rate constants measured in this study emphasize this possibility. Secondly, it clearly motivates the need for further investigation of this chem-

(39) S. P. Sander, M. Peterson, R. T. Watson, and R. Patrick, *J. Phys. Chem.*, **86**, 1236 (1982).
(40) D. L. Baulch, R. A. Cox, P. J. Crutzen, R. F. Hampson, Jr., J. A. Kerr, J. Troe, and R. T. Watson, *J. Phys. Chem. Ref. Data*, **11**, 327 (1982).
(41) U. C. Sridharan, B. Reimann, and F. Kaufman, *J. Chem. Phys.*, **73**, 1286 (1980).
(42) R. F. Hampson, U.S. Department of Transportation, Report No. FAA-EE-80-17, 1980.
(43) H. S. Johnston, "Gas Phase Reaction Rate Theory", Ronald Press, New York, 1966, Chapter 9.
(44) J. O. Hirschfielder, C. F. Curtiss, and R. B. Bird, "Molecular Theory of Gases and Liquids", Wiley, New York, 1964.
(45) R. R. Herm in "Alkali Halide Vapors", P. Davidovits and D. L. McFadden, Ed., Academic Press, New York, 1979, Chapter 6, and references therein.
(46) W. B. Miller, S. A. Safron, and D. R. Herschbach, *J. Chem. Phys.*, **56**, 3581 (1972).
(47) A. Freedman, R. Behrens, Jr., T. P. Parr, and R. R. Herm, *J. Chem. Phys.*, **65**, 4739 (1976).
(48) M. S. Zahniser, F. Kaufman, and J. Anderson, *Chem. Phys. Lett.*, **27**, 507 (1974).

istry, via detailed models, additional laboratory measurements of reaction rate constants and photolysis cross sections, and direct measurement of molecular sodium concentration profiles in the upper atmosphere.

Acknowledgment. The authors thank Drs. F. Kaufman, M. McElroy, and E. Murad for their helpful discussions and insights, and W. Goodwin for his excellent technical assistance. This work was supported by the Chemical Manufacturers Association under Contract No. FC82-401, by the Air Force Geophysics Laboratory under Contract No. F19628-83-C-0010, and by the Army Research Office under Contract No. DAAG29-81-C-0024.

Registry No. NaOH, 1310-73-2; HCl, 7647-01-0.

APPENDIX C

MEASUREMENT OF ATOMIC SODIUM AND POTASSIUM DIFFUSION COEFFICIENTS

Measurement of atomic sodium and potassium diffusion coefficients

Joel A. Silver
Center for Chemical and Environmental Physics, Aerodyne Research, Inc., Billerica, Massachusetts 01821

(Received 30 May 1984; accepted 23 July 1984)

The gaseous diffusion coefficients for sodium and potassium atoms have been measured as a function of temperature in a flow tube. Analysis is based on a simple relationship between diffusion and the observed alkali decay rate for the case of very reactive walls. The resulting values for the diffusion coefficient in units of $cm^2\ s^{-1}$ at 1 atm are:

Na–He	$(2.2 \pm 0.3)\times 10^{-5}\ T^{1.75\pm0.02}$	309–473 K
Na–N_2	$(8.0 \pm 0.8)\times 10^{-6}\ T^{1.79\pm0.02}$	320–698 K
Na–Ar	$(1.2 \pm 0.9)\times 10^{-5}\ T^{1.71\pm0.11}$	322–350 K
K–He	$(1.5 \pm 1.0)\times 10^{-4}\ T^{1.48\pm0.19}$	301–734 K
K–N_2	$(4.5 \pm 2.8)\times 10^{-5}\ T^{1.54\pm0.09}$	302–720 K

The results agree well with previous measurements and the comparison with theoretical expectations is discussed.

I. INTRODUCTION

The transport properties of gases are important in investigating the details of atomic and molecular interaction potentials and in a more practical sense, are needed to describe the dynamics of flow and reaction in natural and industrial processes. Our interest in diffusion coefficients stems from the need to correct flow tube kinetic rate data for wall and diffusional effects.

Measurements of diffusion coefficients of alkali atoms date back to the early 1930's. Since then, a variety of experimental approaches have been used, including static diffusion cells,[1] spin relaxation,[2–5] pulsed irradiation,[6–8] flame photometry,[9–12] resonance ionization spectroscopy,[13,14] and sophisticated digital correlation techniques.[15] The results reported in this paper are obtained from the observed decay of laser induced alkali atom fluorescence in a flowing gas in a regime where wall loss is very efficient and axial diffusion unimportant. The techniques discussed in analyzing the data are a special case of the more general solution used in correcting observed bimolecular reaction rate constants for the effects of wall removal and diffusion in a flow tube.[16–19] In this work, the bimolecular reaction rate is zero, and the solution is somewhat simplified.

II. EXPERIMENTAL

A. Apparatus

The high temperature fast flow reactor used in these experiments has been described in detail previously.[20] Briefly, a 7.26 cm diameter, 120 cm long alumina tube is heated with Kanthal resistance heaters capable of maintaining uniform temperatures in the reaction zone. The helium, argon or nitrogen carrier gas enters the flow tube through two mullite multichannel arrays which both preheat and laminarize the flow upstream of the reaction zone. A sufficient distance is allowed downstream of these arrays for the carrier gas to develop a parabolic flow profile before reaching the reaction zone. The gas is pumped by a 450 $l\ s^{-1}$ Roots blower and mechanical fore pump combination. Linear flow velocities from 220 to 2800 cm s^{-1} are used in the present experiments. Carrier gas flow rates from 30 to 400 STP $cm^3\ s^{-1}$ are measured with calibrated rotameters. Total pressure is measured with a capacitance manometer at the downstream end of the reaction zone. Gas temperatures are obtained with a chromel–alumel thermocouple which is movable throughout the reaction zone. Although the apparatus is capable of temperatures up to 1500 K, experimental considerations as described below limited the upper temperature to 700 K for these studies.

For nominal room temperature measurements (flow tube wall heaters off), the axial temperature profile is not uniform, but exhibits a small drop in temperature downstream of the alkali oven. Gas passing by or through the oven is heated, and then cools as it travels further down the tube. Over the region in which decay measurements are taken, the maximum variation from the average temperature is typically five to ten degrees, depending on the flow velocity, total pressure, and identity of the carrier gas. The more important effect is that the average gas temperature is 15° to 25° warmer than room temperature, and is the correct value to use in analyzing the data. At elevated temperatures (> 400 K), gas heating is dominated by the walls and mullite arrays, and the oven contribution is secondary. As a result, the axial profiles are more uniform, with variations of only 2°–5°.

Alkali atoms are generated by heating the pure metal in a 25 mm diam cylindrical silver plated monel oven to a temperature sufficient to obtain a vapor pressure of 10^{-6} to 10^{-4} Torr within the oven. The oven is mounted on the end of a movable 13 mm o.d. alumina tube concentric to the main flow tube. The vapor is entrained in a flow of carrier gas and introduced into the flow tube in one of two configurations. In the first, the oven is placed at a fixed position upstream of the multichannel arrays. The alkali vapor is introduced into the main flow through a 10 cm length of 19 mm o.d. silver tubing which passes through the center of the arrays. In the second configuration, the oven is placed downstream of the arrays and is movable throughout the reaction zone. The oven temperature is controlled with resistive heating elements independent of the flow tube heaters. Initial alkali atom concentrations in the reaction zone are maintained at less than 10^{10}

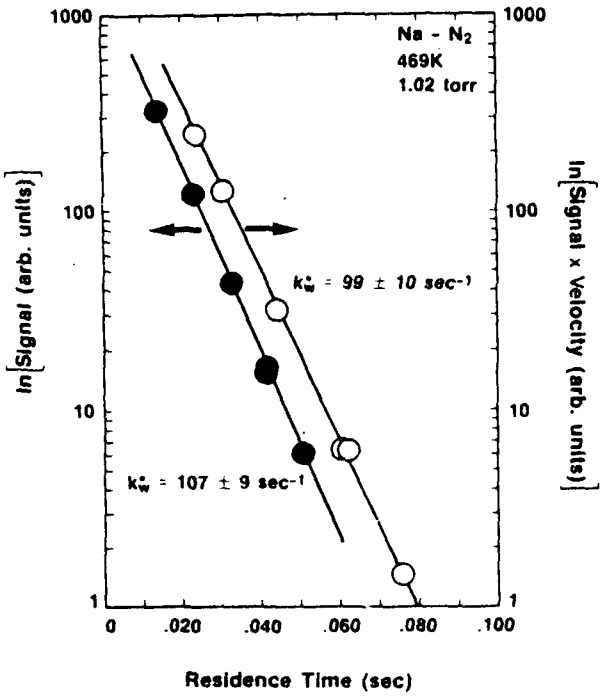

FIG. 1. Typical decay plots of Na using fixed and moveable source methods. Both runs were made at 469 K in 1.02 Torr N_2. (a) Movable source; $\langle u \rangle = 1080\,\mathrm{cm\,s^{-1}}$, $z = 15$–65 cm. (b) Fixed source; $z = 65$ cm, $\langle u \rangle = 850$–$2750\,\mathrm{cm\,s^{-1}}$.

cm^{-3} by adjusting the oven temperature and the carrier gas flow rate through the oven.

The alkali atoms are detected by laser induced fluorescence at the downstream end of the flow tube. A Molectron DL14 nitrogen pumped dye laser is used to excite the $4s\ ^2S_{1/2} \rightarrow 5p\ ^2P_{3/2}$ transition at 404.4 nm for potassium and the $3s\ ^2S_{1/2} \rightarrow 3p\ ^2P_{3/2}$ transition at 589.0 nm for sodium. Fluorescence is collected using a gated phototube and a computer controlled data acquisition system.[20] The signals are averaged over 100 laser pulses after subtracting nonfluorescent background contributions and normalizing for pulse to pulse fluctuations in laser intensity. To verify that the transitions were not saturated and that the samples were optically thin, it was observed that the measured fluorescence varied linearly with both alkali number density and laser intensity. Although no direct calibration of the fluorescence signal was attempted, estimates of sensitivity from known phototube and integrator responses, measured laser power, and atomic transition probabilities indicate a detection limit for Na of $10^4\ \mathrm{cm}^{-3}$ and for K of $10^6\ \mathrm{cm}^{-3}$ using these transitions.

Loss of atoms on the walls as a function of residence time in the flow tube is measured in two ways. The oven position z is varied at fixed average flow velocity $\langle u \rangle$. The observed decay rate k_w^* is equal to the slope of ln (signal) vs time $(z/\langle u \rangle)$. The second method uses the fixed alkali source. Here the residence time is varied by changing the flow velocity, with the pressure constant, so that the diffusion coefficient is the same for all measurements. A plot of ln (signal·$\langle u \rangle$) vs time gives a slope equal to k_w^*. The velocity term in the ordinate is required to compensate for the change in alkali density in the detector due to dilution by the increased carrier gas flow as the velocity is changed. This latter technique is often useful when it is difficult to use a movable source. Comparison of the two methods shows no significant difference in the final observed rate constants under the conditions present in this work. An example of results for both types of measurements under the same pressure and temperature conditions is shown in Fig. 1. Decays are very linear and exhibit little scatter. Most of the measurements for Na were made using the variable distance method, while all of the K runs used a fixed distance of 73 cm. At temperatures above 700 K, alkali atoms were observed to effuse from the walls, as evidenced by nonzero signals with the oven entrainment flow turned off. As a result, no data were taken above this temperature.

B. Analysis

Data analysis is based on the solution to the diffusion equation for laminar, Poiseuille flow in a cylindrical tube in which the only loss process is by heterogeneous removal at the wall.[16,18] This equation is expressed in terms of the tube radius a, radial distance r, axial distance z, species concentration C, diffusion coefficient D_c, and mean velocity $\langle u \rangle$ as

$$2\langle u \rangle \left(1 - \frac{r^2}{a^2}\right)\frac{\partial C}{\partial z} = D_c\left(\frac{\partial^2 C}{\partial r^2} + \frac{1}{r}\frac{\partial C}{\partial r} + \frac{\partial^2 C}{\partial z^2}\right). \quad (1)$$

Note that this contains both axial and radial diffusion terms. The first order rate constant for wall removal k_w appears in the boundary condition

$$D_c\left[\frac{\partial C}{\partial r}\right]_{r=a} = -\frac{k_w a C_{r=a}}{2}. \quad (2)$$

These equations can be rewritten in terms of dimensionless parameters as

$$(1 - R^2)\frac{\partial C}{\partial Z} = D\left(\frac{\partial^2 C}{\partial R^2} + \frac{1}{R}\frac{\partial C}{\partial R} + \frac{\partial^2 C}{\partial Z^2}\right), \quad (3)$$

with

$$D\left(\frac{\partial C}{\partial R}\right)_{R=1} = -\frac{K_w C_{R=1}}{2}, \quad (4)$$

where $R = r/a$, $Z = z/a$, $D = D_c/2a\langle u \rangle$, and $K_w = k_w a/2\langle u \rangle$. Furthermore, γ, the collision efficiency for wall loss of C (also called the sticking coefficient), is related to k_w by elementary kinetic theory[21]

$$k_w = \frac{\bar{c}\gamma}{2a(1 - \gamma/2)}, \quad (5)$$

where $\bar{c}$ is the mean molecular velocity of C.

Although the exact solution of Eq. (3), subjected to the boundary conditions, can be obtained only by numeric methods, it can be solved[16–18] by assuming a solution of the form

$$C = \sum_{i=1}^{\infty} A_i\, g_i(R)\, e^{-K_i^* Z}. \quad (6)$$

Substitution of this into Eqs. (3) and (4) leads to an infinite set of ordinary differential equations

$$\frac{d^2 g_i(R)}{dR^2} + \frac{1}{R}\frac{dg_i(R)}{dR} + \left[K_i^{*2} + (1 - R^2)K_i^*/D\right] g_i(R) = 0 \quad (7)$$

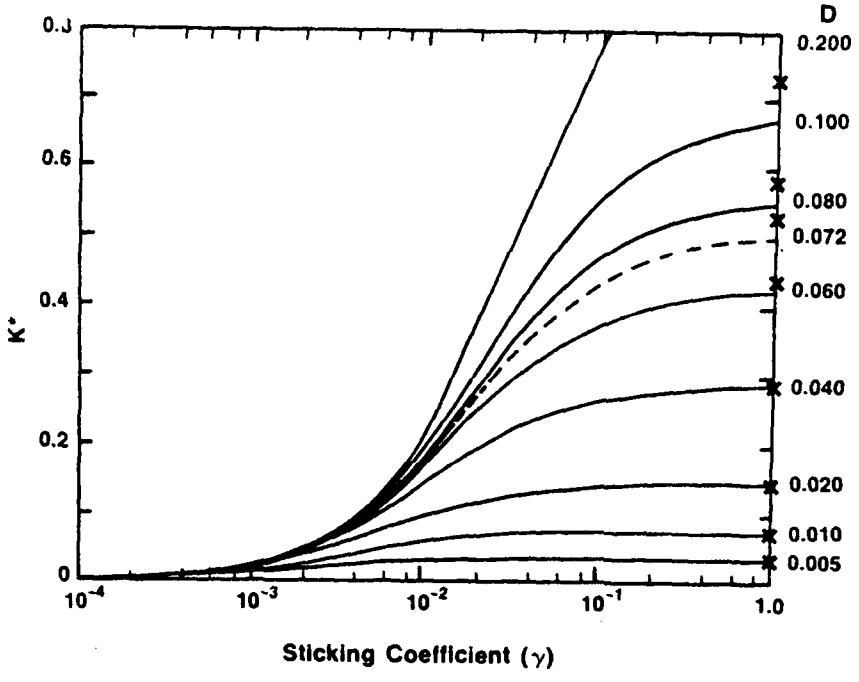

FIG. 2. Observed decay rate (k_w^*) vs sticking coefficient for a series of diffusion coefficients. The dashed line corresponds to the situation where axial and radial effects are equal. The symbols (x) on the right-hand axis corresponds to k_w^* calculated using Eq (15).

and

$$\left[\frac{dg_i(R)}{dR}\right]_{R=1} = -\frac{K_w\, g_i(R)_{R=1}}{2D}. \tag{8}$$

It is found that $g_i(R)$ can be expressed as a series in even powers of R (dropping the subscripts for clarity)

$$g(R) = \sum_{n=0}^{\infty} B_n R^{2n}, \tag{9}$$

with coefficients

$$B_0 = 1, \tag{10}$$

$$B_1 = -\frac{\alpha B_0}{4}, \tag{11}$$

and

$$B_n = \frac{1}{(2n)^2}\left[\left(\frac{K^*}{D}\right)B_{n-2} - \alpha B_{n-1}\right], \tag{12}$$

where

$$\alpha = K^{*2} + \frac{K^*}{D}. \tag{13}$$

Substitution of Eq. (9) into the boundary condition (8) leads to the expression (for each i)

$$\sum_{n=0}^{\infty} B_n\left(2n + \frac{K_w}{2D}\right) = F(K_w, K^*, D) = 0. \tag{14}$$

If K_w and D are specified, then the first positive root of F is K_1^*, the second root is K_2^*, and higher roots become K_3^*, K_4^*, etc. For sufficiently large values of Z, the higher order terms in Eq. (6) rapidly decay, so that the observed disappearance of C is described by a single exponential term ($i = 1$), with the corresponding decay rate K^* related to the observed decay rate k_w^* (s^{-1}) such that $K^* = ak_w^*/\langle u\rangle$.

Figure 2 illustrates the relationship between K^* (observed wall loss rate constant) and the sticking coefficient γ as a function of the diffusion parameter D for sodium at 300 K. As shown in this figure, for smaller values of D, the K^* curve flattens as γ approaches unity. For $\gamma > 0.1$, K^* is independent of γ and varies linearly with D. These phenomena

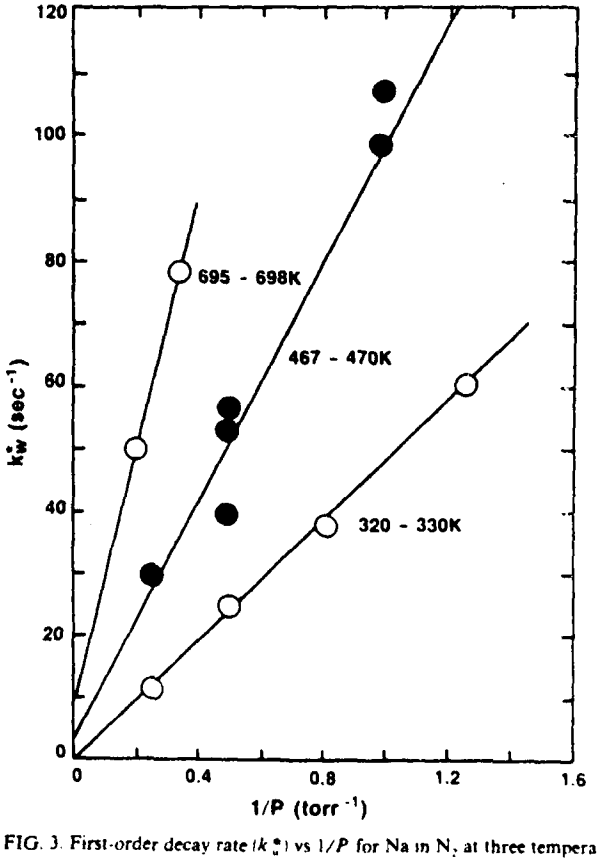

FIG. 3. First-order decay rate (k_w^*) vs $1/P$ for Na in N_2 at three temperatures.

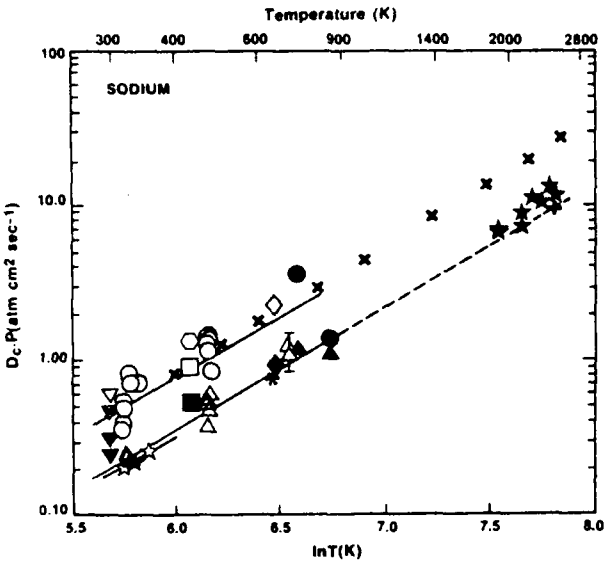

FIG. 4. Diffusion coefficients for sodium as a function of temperature. Experimental data in helium are shown for this work (○), Fairbank *et al.* (Ref. 15) (▽), Husain and Plane (Ref. 6) (●), Ramsey and Anderson (Ref. 2) (□), and Hartel *et al.* (Ref. 1) (◇), and Bichi *et al.* (Ref. 3) (○); in nitrogen for this work (△), Husain and Plane (Ref. 6) (▲), Ramsey and Anderson (Ref. 2) (■), and Hartel *et al.* (Ref. 1) (◆); in argon for this work (☆), Fairbank *et al.* (Ref. 15) (▼), and Hartel *et al.* (Ref. 1) (✱); in flames for Ashton and Hayhurst (Ref. 10) (★) and Snelleman (Ref. 12) (+). The crosses (×) correspond to calculations of Redko (Ref. 26) in helium, and the solid lines the best fits to the present data. The dashed line is an extrapolation of the fit in N_2 to flame temperatures.

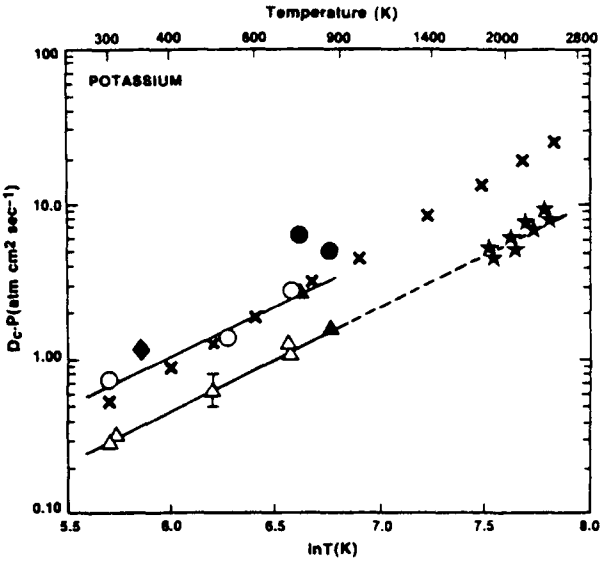

FIG. 5. Diffusion coefficients for potassium as a function of temperature. Experimental data in helium are shown for this work (○), Bernheim and Korte (Ref. 5) (◆), and Husain and Plane (Ref. 7) (●); in nitrogen for this work (△) and Husain and Plane (Ref. 7) (▲); in flames for Hayhurst and Ashton (Ref. 11) (✱). The crosses (×) correspond to calculations of Redko (Ref. 26) in helium and the solid lines the best fits to the present data. The dashed line is an extrapolation of the fit in N_2 to flame temperatures.

occur when the decay of C is controlled by radial diffusion. The effects of axial and radial diffusion become equal at $D = 0.072$ and axial diffusion dominates at larger values of D. Ferguson *et al.*[19] have shown that in the limit of unit wall loss ($\gamma = 1$) and radial diffusion control,

$$D = 0.137\,K^*. \tag{15}$$

The symbols (X) on the right-hand axis of Fig. 2 represent K^* calculated for the given values of D using this formula. Agreement between these and the exact solutions are quite good in the radial diffusion limit ($D<0.05$).

III. RESULTS

A total of 29 wall loss measurements were made for sodium and eight for potassium between 300 and 700 K. At each temperature, runs were made at a number of different pressures in the range of 1–8 Torr. All runs were in the radial diffusion limit. Since alkali atoms are removed by the uncoated alumina flow tube walls with near unit efficiency, diffusion coefficients were directly obtained from the observed decay rates using a computer program based on the derivation in Sec. II B. It is assumed that $\gamma = 1$, but even if $\gamma = 0.2$, the error in D_c would be $< 5\%$. The assumption of $\gamma = 1$ is further confirmed by observing that since D_c is inversely proportional to pressure, a plot of k_u^* vs $1/P$ for a given buffer gas and temperature will be linear only in the limit of $\gamma \to 1$. An example of this linearity is seen in Fig. 3 for Na in N_2 at three different temperatures.

As mentioned in Sec. II B, it was assumed that Poiseuille flow exists in the measurement region and that only the first term of Eq. (6) is significant. For parabolic flow to be *fully developed, an inlet mixing length* of approximately $R_e d/20$ is required,[22] where R_e is the flow Reynold's number and d the tube diameter. In all experiments this distance is < 20 cm, permitting a minimum of 65 cm for measuring decay rates.

The second requirement is that the decay of C be described by a single exponential term. This requires calculation of the A_i and $g_i(R)$ terms in Eq. (6). Following the procedure of Pirkle and Sigillito,[17] the first eight terms of $C(r,z)$ were calculated. Initial conditions accurately reflected the true source inlet geometry, rather than assuming an initial uniform concentration profile of C across the entire flow tube as done by Pirkle. The results show that the sum of all higher order modes decay to less than 5% of the first term in less than 10 cm. Furthermore, no curvature was observed in the decay data at shorter reaction times as might be expected if higher order terms were significant (Fig. 1).

Diffusion coefficients resulting from these experiments are shown in Fig. 4 for sodium and Fig. 5 for potassium. The data (including their associated uncertainties) have been fit to a functional form $D_c = aT^n$ using a nonlinear least square analysis. The best fit coefficients are shown in Table I and the solid lines in Figs. 4 and 5 represent these fits. The expressed total experimental uncertainties for each D_c, including allowance for systematic errors, can be estimated as the square root of the sum of the squared individual uncertainties due to (a) flow velocity, temperature, and pressure calibration factors, 7.2%, (b) the precision in determining the coefficients a and n in the expression for D_c, 5.4%, and (c) the uncertainty in converting K^* to D_c, 5%.

TABLE I. Comparison of experimental values of diffusion coefficients for sodium and potassium.

Alkali	Buffer gas	T(K)	D_c ($cm^2 s^{-1}$ at 1 atm; $\pm 1\sigma$)	Method	Reference
Na	He	309–473	$(2.2 \pm 0.3)\times 10^{-5}\ T^{1.75\pm0.02}$	Flow tube	This work
	N_2	320–698	$(8.0 \pm 0.8)\times 10^{-6}\ T^{1.79\pm0.02}$		
	Ar	322–350	$(1.2 \pm 0.9)\times 10^{-5}\ T^{1.71\pm0.11}$		
Na	He	724,844	3.58 ± 0.09, 1.36 ± 0.11 (2σ)	Pulse irradiation/ resonance absorption	Husain and Plane (Ref. 6)
	N_2	724,844	1.17 ± 0.04, 1.14 ± 0.05 (2σ)		
	CO_2	724,844	4.96 ± 0.04, 1.63 ± 0.05 (2σ)		
Na	He	300	0.474 ± 0.120, 0.564 ± 0.126 (3σ)	Laser beam transit times	Fairbank *et al.* (Ref. 15)
	Ar	300	0.258 ± 0.053, 0.329 ± 0.080 (3σ)		
Na	He	453	1.2 ± 0.2	Spin relaxation	Bicchi *et al.* (Ref. 3)
	Ne	453	0.67 ± 0.05		
^{20}Na	Ne	300	0.35 ± 0.08	Pulsed irradiation/ resonance fluorescence	Coolen and Hagedoorn (Ref. 8)
Na	H_2	473	1.3	Spin relaxation	Ramsey and Anderson (Ref. 2)
	He	428	0.92		
	Ne	428	0.50		
	N_2	453	0.54		
Na	H_2	655	3.14	Static diffusion cell	Hartel *et al.* (Ref. 1)
	He	654	2.17		
	N_2	655	0.91		
	Ar	654	0.88		
	C_5H_{12}	655	0.23		
Na	$C_2H_2/O_2/N_2$ Flame products	2440	9.9 ± 0.5	Flame photometry[a]	Snelleman (Ref. 12)
Na	$H_2/O_2/N_2$ Flame products	1920–2520	$9.3\times 10^{-7}\ T^{2.1}$	Flame photometry[b]	Ashton and Hayhurst (Ref. 10)
K	He	301–724	$(1.5 \pm 1.0)\times 10^{-4}\ T^{1.48\pm0.19}$	Flow tube	This work
	N_2	302–720	$(4.5 \pm 2.8)\times 10^{-5}\ T^{1.54\pm0.09}$		
K	He	753,873	6.41 ± 0.41, 4.97 ± 0.34(2σ)	Pulse irradiation/ resonance absorption	Husain and Plane (Ref. 7)
	N_2	753,873	2.70 ± 0.18, 1.54 ± 0.11(2σ)		
	CO_2	753,873	4.49 ± 0.41, 1.37 ± 0.34(2σ)		
K	$H_2/O_2/N_2$ Flame products	1900–2520	$3.1\times 10^{-7}\ T^{2.2}$	Flame photometry[c]	Ashton and Hayhurst (Ref. 11)
K	He	358	1.2	Spin relaxation	Bernheim and Korte (Ref. 5)

[a] Ashton reports the results of Snelleman to have a $T^{1.75}$ temperature dependence although no range of temperatures is specified.
[b] Average of eight data points fit to an expression of the form aT^n. Individual data are shown in Fig. 4.
[c] Average of eight data points fit to an expression of the form aT^n. Individual data are shown in Fig. 5.

IV. DISCUSSION

The results presented here compare well with previous measurements for sodium and potassium (Table I) and span a wide temperature range, permitting an accurate determination of the temperature dependence of D_c. Despite the variety of different techniques used, the data agree well over a 2000 K temperature range, based on an extrapolation of our temperature dependences. More recent measurements include those of Ashton and Hayhurst,[10,11] who measured the diffusion of alkali atoms (Na, K, Cs, Rb) and LiOH in $H_2/O_2/N_2$ flames, introduced from a point source. The data for Na and K match the extrapolated N_2 fits very well, as might be expected since the flame products are 54%–75% N_2, the balance being mostly H_2O with some (1%–10%) H_2.[9] Husain and Plane[6,7] obtained diffusion coefficients in a pulsed irradiation cell, reporting substantially different results at the two temperatures used. Their lower temperature data (724 and 753 K for Na and K, respectively) appear to be anomalously high, but no reason for this is given. Fairbank *et al.*,[15] in contrast to this and all of the other work, use a much different approach to measure D_c. Transit time measurements of a single atom across a laser beam are computed from the observed photon burst signal. In these experiments, the atom absorbs and reemits the resonance laser radiation many times and the time dependent signal is treated by digital correlation techniques to provide the mean traversal time and thus the diffusion coefficient.

The calculation of D_c from transport theory has been well described.[23] Given the interaction potential energy sur-

face for the diffusing species and the buffer gas, D_c can readily be calculated. In the absence of experimental data, approximations using simplified potentials such as a Lennard-Jones often lead to values of D_c accurate to within a factor of 2. For the alkali atom-rare gas systems, more detailed interaction potentials are now available,[24,25] and Redko[26,27] has used them to calculate diffusion integrals and coefficients for ground and excited electronic states of Na and K in rare gases over the temperature range 300 to 3000 K. His results for Na($3\,^2S$) and K($4\,^2S$) in He are shown as crosses (x) in Figs. 4 and 5, respectively, and show remarkably good agreement with the experimental results over the temperature range studied, including the different temperature dependence of D_c between Na and K.

The measurements of diffusion coefficients in our laboratory are presently being extended to include molecular alkali species. Preliminary results for NaOH in He at 308 K are 0.47 ± 0.05 and 0.4 ± 0.1 cm^2 s^{-1} for NaCl in He at 1 atm.

ACKNOWLEDGMENTS

The author would like to thank Dr. M. Zahniser for many helpful discussions and W. Goodwin for his excellent technical assistance. This work was supported by the Air Force Geophysics Laboratory under Contract No. F19628-83-C-0010 and by the Chemical Manufacturers Association under Contract No. FC82-401.

[1]H. V. Hartel, N. Meer, and M. Polanyi, Z. Phys. Chem. **199**, 139 (1932).
[2]A. T. Ramsey and L. W. Anderson, Nuovo Cimento **32**, 1151 (1964).
[3]P. Bichi, L. Moi, P. Savino, and B. Zambon, Nuovo Cimento B **55**, 1 (1980).
[4]A. Gozzini, N. Ioli, and F. Strumia, Nuovo Cimento B **49**, 185 (1967).
[5]R. A. Bernheim and M. W. Korte, J. Chem. Phys. **42**, 2721 (1965).
[6]D. Husain and J. M. C. Plane, J. Chem. Soc. Faraday Trans. 2 **78**, 163 (1982).
[7]D. Husain and J. M. C. Plane, J. Chem. Soc. Faraday Trans. 2 **78**, 1175 (1982).
[8]F. C. M. Coolen and H . L. Hagedoorn, Physica C **79**, 402 (1975).
[9]A. F. Ashton and A. N. Hayhurst, Trans. Faraday Soc. **66**, 824 (1970).
[10]A. F. Ashton and A. N. Hayhurst, Trans. Faraday Soc. **66**, 833 (1970).
[11]A. F. Ashton and A. N. Hayhurst, J. Chem. Soc. Faraday Trans. 2 **69**, 652 (1973).
[12]W. Snelleman, Thesis, Utretcht, 1965.
[13]I. W. Grossman, G. S. Hurst, S. D. Kramer, M. G. Payne, and J. P. Young, Chem. Phys. Lett. **50**, 207 (1977).
[14]G. S. Hurst, S. L. Allman, M. G. Payne, and T. J. Whitaker, Chem. Phys. Lett. **60**, 150 (1978).
[15]W. M. Fairbank, Jr., C. Y. She, and J. V. Prodan, SPIE **186**, 94 (1981).
[16]R. L. Brown, J. Res. Natl. Bur. Stand. **83**, 1 (1978).
[17]J. C. Pirkle, Jr. and V. G. Sigillito, Int. J. Eng. Sci. **10**, 553 (1972).
[18]R. E. Walker, Phys. Fluids **4**, 1211 (1961).
[19]E. E. Ferguson, F. C. Fehsenfeld, and A. L. Schmeltekopf, Adv. At. Mol. Phys. **5**, 1 (1969).
[20]M. E. Gersh, J. A. Silver, M. S. Zahniser, C. E. Kolb, R. B. Brown, C. M. Gozewski, S. Kallelis, and J. C. Wormhoudt, Rev. Sci. Instrum. **52**, 1213 (1981).
[21]P. G. Dickens, D. Schofield, and J. Walsh, Trans. Faraday Soc. **56**, 225 (1960).
[22]W. M. Kays, *Convective Heat and Mass Transfer* (McGraw-Hill, New York, 1966), p. 63.
[23]J. O. Hirschfelder, C. F. Curtiss, and R. B. Bird, *Molecular Theory of Gases and Liquids* (Wiley, New York, 1954).
[24]J. Pascale and J. Vandeplanque, J. Chem. Phys. **60**, 2278 (1974).
[25]J. Hanssen, R. McCarroll, and P. Valiron, J. Phys. B **12**, 899 (1979).
[26]T. P. Redko, Opt. Spectrosc. (USSR) **52**, 461 (1982).
[27]T. P. Redko, Sov. Phys. Tech. Phys. **28**, 1065 (1983).